Journal of Computational Physics (2019)
Contents lists available at ScienceDirect
Journal of Computational Physics
journal homepage: www.elsevier.com/locate/jcp

Self-induced temperature correction for inter-phase heat transfer in Euler-Lagrange point-particle simulation

Kai Liu[a], Mandar Lakhote[a], S. Balachandar[a,*]

[a]*Department of Mechanical & Aerospace Engineering, University of Florida, Gainesville, FL, 32611, USA*

ARTICLE INFO

Article history:
Received
Received in final form
Accepted
Available online

Communicated by

ABSTRACT

In a two-way coupled Euler-Lagrange simulation, particles are approximated as point sources and their momentum and energy exchange with the surrounding flow are modeled through point-particle force and heat transfer models. As the particle size increases and approaches the Eulerian grid, the feedback force and heat transfer become large and strongly affect the local flow at the particle location. The fluid velocity and temperature computed in the EL simulation when interpolated to the particle location will be substantially different from the corresponding undisturbed values. In this work we will follow the approach pursued in Balachandar *et al.* (2018)[1] for self-induced velocity correction to develop an analogous correction procedure for self-induced temperature. We obtain analytical solutions for the self-induced thermal perturbation for a steady uniform cross flow past a Gaussian filtered heat source under both steady and unsteady conditions. The analytical results are extended to finite Peclet number using numerical simulations. The resulting quasi-steady and unsteady models are tested with a simple problem of exponential thermal evolution against the corresponding EL simulation results. We also provide a simple criterion for when the self-induced temperature correction is needed in an Euler-Lagrange simulation.

*Corresponding author: Tel.: +1-352-392-8909; fax: +1-352-392-1703;
e-mail: balals@ufl.edu (S. Balachandar)

1. Introduction

The Euler-Lagrange (EL) point-particle approach has been widely implemented in multiphase flows involving heat and mass transfer (e.g. [2, 3, 4, 5, 6]). Fluidized beds, liquid droplet evaporation and spray combustion are some salient examples. Since each particle is approximated as a point mass, the surrounding microscale flow that varies on the particle scale is not resolved. Drag force and heat transfer models are used in evolving the position, velocity and thermal state of the particles. As a result, precise closure models for the drag force and heat transfer are essential to guarantee simulation accuracy. In two-way coupled simulations, the drag force and heat transfer are fed back to the fluid as point sources of momentum and energy. To accomplish this and to avoid any singularity, the feedback force and heat source are either spread over the nearby finite volume cells or multiplied with a Guassian filter before being projected onto the fluid field [7]. Note that there are other filter function such as trilinear and polynomial functions have also being used depending on the type of flow and the particle size.

Historically the EL methodology with the point-particle models has been applied mainly to systems where (i) the particles are much smaller than the size of the Eulerian grid used in the flow simulation, and (ii) the volume fraction of particles is reasonably small [8]. These restrictions are important as they allow the use of standard drag laws and heat transfer coefficients that were developed for an isolated particle subjected to a uniform flow [9]. At low volume fraction, the influence of other particles can be ignored. And for a particle much smaller than the grid, the local ambient flow can be approximated as nearly uniform. Furthermore, with the restriction to small particles, the flow properties at the particle position can be easily computed through interpolation from nearby grid points and also the particle force and heat transfer can be easily fed back to the fluid.

These restrictions however limited the applicability of the EL methodology. In the past decade there have been many attempts where these restrictions have been relaxed and the EL methodology has been applied for larger particles of size comparable to the grid [10, 11, 12] and to systems of large particle volume fraction [13, 14, 15, 16]. In doing so, an important modeling challenge has recently been recognized, which can be stated as follows. As the particle size increases and approaches the Eulerian grid, the feedback force becomes large and strongly affects the local flow at the particle location. The fluid velocity computed in the EL simulation when interpolated to the particle location will be substantially different from the fluid velocity that would exist in the absence of the particle. In other words, the *disturbed fluid velocity* computed with the feedback force from the particle and the *undisturbed fluid velocity* computed ignoring the feedback force will differ substantially. The difference between the two is due to the application of the feedback force of that particle. While the disturbed velocity is the only quantity available in an EL simulations, all the available point-particle drag models are based on the undisturbed fluid velocity. If we were to compute the force on the particle using these point-particle drag laws, but with the disturbed velocity instead of the undisturbed velocity at the particle, the resulting force on the particle is in substantial error. Several approaches to reducing this error by correcting the disturbed fluid velocity and backing out the undisturbed velocity in an EL simulation have been proposed [17, 10, 18, 19, 11, 12, 1, 20, 21].

In this work we will address an identical problem that exists in the context of heat transfer, which can be stated as follows. In an EL simulation, when a particle becomes large and approaches the size of the local grid, the associated heat transfer to the surrounding fluid will be strong. When this back coupling to the fluid is applied as a strong local heat source/sink, the *disturbed temperature* value computed in the EL simulation at the particle position will substantially differ from the *undisturbed temperature* that would have resulted in the absence of the heat source/sink from that particle. Again the difference between the disturbed and the undisturbed thermal fields is referred to as self-induced perturbation due to the thermal feedback from the particle. The purpose of this paper is to develop a correction procedure that can be applied in a EL simulation in order to extract the undisturbed fluid

temperature at the particle position from the computed disturbed thermal field.

In a thermal point-particle model, inter-phase heat transfer is expressed as the summation of three physically meaningful contributions: quasi-steady heat transfer Q_{qs}, undisturbed-unsteady heat transfer Q_{uu} and diffusive-unsteady heat transfer Q_{du} [9]. The latter two terms together can be referred to as unsteady heat transfer because they are nonzero only when the time rate of temperature change is nonzero. An accurate and efficient prediction model for the self-induced temperature is needed in order to compute the quasi-steady heat transfer between the particle and the fluid, which is usually the dominant component of heat transfer.

In this work we will follow the approach pursued in [1] for self-induced velocity correction to develop an analogous correction procedure for self-induced temperature. In the sense the present paper can be considered part two, with the referenced [1] being the part one of the correction to self-induced perturbation. We will consider a steady uniform cross flow and a Gaussian filtered heat source under both steady and unsteady conditions in a frame attached to the particle. First, in the low Peclet number limit we will use Oseen's approximation to derive an exact steady state solution for the self-induced temperature perturbation at the particle location. The analytical solution will then be empirically extended to finite Peclet number using numerical solutions. In the unsteady regime, an exact solution will be obtained in the Stokes limit for a single particle subjected to an oscillatory heat flux. The unsteady problem in the finite Peclet number regime is then studied using numerical simulations. These results are then used to obtain a convolution integral, which together with the quasi-steady model provides an unsteady self-induced temperature correction model. The model is finally tested in a simple test case of exponential thermal evolution and the predictions of the steady and unsteady models are compared against the corresponding EL simulation results.

In summary, the primary goals of the paper are to (i) establish conditions under which a correction to self-induced thermal perturbation is warranted, (ii) obtain a concise and accurate quasi-steady model for the thermal correction that is applicable over a wide range of Reynolds and Prandtl numbers, (iii) extend the quasi-steady model to include unsteady effects, and (iv) investigate the interaction between momentum and energy coupling.

The organization of this paper is as follows. In Section 2 we present the analytical solution of the volume weighted energy equation in the Stokes limit (the derivation of the Oseens solution is shown in Appendix A.). In Section 3 we elaborate the numerical methodology and simulation setup to be employed. In Sections 4 and 5 the finite Peclet number steady and unsteady thermal correction models are introduced respectively. The result of the application of the model to a simple test problem is shown in Section 6, followed by discussion and conclusion in Sections 7 and 8.

2. Mathematical Formulation

This section will begin with a description of the governing equations of an isolated particle within an isothermal uniform ambient flow in a two-way coupled Euler-Lagrange simulation. Here, by subjecting the particle to a temperature different from that of the ambient fluid, we mainly focus on the energy equation. Our goal is to evaluate the self-induced temperature perturbation due to the feedback of heat transfer to the fluid as a heat source/sink. An analytical solution will be obtained to the unsteady problem in the Stokes limit. The correction model derived from investigating an isolated particle can then be applied to EL simulations involving many particles.

In the lab frame, consider a rigid spherical particle of diameter d_* with velocity $-\mathbf{U}_*(t_*)$ moving in a quiescent fluid. While the temperature of the far-field fluid is maintained as a constant at T_{f*}, the particle temperature can be time-dependent and is specified as $T_{p*}(t_*)$. An important assumption made here is that the particle Biot number is sufficiently small that the temperature variation inside the particle can be ignored, which is an implicit assumption in many Euler-Lagrange simulations.

By changing to a non-inertial frame attached to the particle center and assuming the fluid to be incompressible, the governing equations of the flow outside the particle can be expressed as

$$\nabla_* \cdot \mathbf{u}_* = 0\,, \tag{1}$$

$$\frac{\partial \mathbf{u}_*}{\partial t_*} + \mathbf{u}_* \cdot \nabla_*(\mathbf{u}_*) = \frac{d\mathbf{U}_*}{dt_*} - \frac{1}{\rho_*}\nabla_* p_* + \nu_* \nabla_*^2 \mathbf{u}_*\,, \tag{2}$$

$$\frac{\partial T_*}{\partial t_*} + \mathbf{u}_* \cdot \nabla_*(T_*) = \alpha_* \nabla_*^2 T_*\,, \tag{3}$$

where the asterisk subscript means the variable is dimensional. In the above $\mathbf{u}_*$, p_*, T_* are the Eulerian fluid velocity vector, pressure and temperature fields, respectively and ρ_*, ν_*, and α_* are the fluid density, kinematic viscosity, and thermal diffusivity, respectively. In this frame of reference, the particle is stationary and the far-field velocity is $\mathbf{U}_*(t_*)$. In the momentum equation (2), the first term on the right is the acceleration of the frame attached to the particle. Also note that the particle temperature T_{p*} is used as the reference. Therefore, T_{f*} denotes the fluid temperature relative to the particle temperature throughout the further discussions.

In a fully resolved DNS, the above governing equations are solved with no-slip, no-penetration, and thermal boundary conditions at the particle surface. From the solution, the tractional force and interphase heat transfer are accurately calculated through surface integration. However, in a two-way coupled Euler-Lagrange point-particle simulation, the particle is taken as a point source of momentum and heat in the fluid momentum and energy equations without imposing specific conditions at the physical interphase boundary. Instead of resolving the momentum and thermal boundary layers around the particle, a Gaussian smoothing is applied to project the total tractional force and heat flux onto the Eulerian grid. Through this Gaussian spreading, the fluid flow is perturbed by the presence of the particle. Of particular interest here is the fact that as a result of this perturbation, the fluid velocity $[\mathbf{u}_*]_p$ and temperature $[T_*]_p$ at the point particle position will deviate from the corresponding undisturbed ambient values of $\mathbf{U}_*$ and T_{f*}. The difference between the particle center values obtained in an EL simulation and the corresponding undisturbed ambient values are referred to as self-induced perturbation velocity and temperature as

$$[\mathbf{u}'_*]_p = [\mathbf{u}_*]_p - \mathbf{U}_* \quad \text{and} \quad [T'_*]_p = [T_*]_p - T_{f*}\,. \tag{4}$$

While the standard point-particle models have been derived and applied based on the undisturbed relative velocity and temperature, in a real implementation of the two-way coupled Euler-Lagrange simulation, only the disturbed fluid velocity and temperature fields are being solved, and available for interpolation to the particle center. In this way, the self-induced perturbation effects are inevitably included and sometimes large enough to result in substantial error when estimating the drag force or heat flux between the particle and the surrounding fluid. Therefore, in the application of the point particle models the correct procedure is to accurately evaluate the self-induced velocity and temperature perturbations and apply these corrections to obtain the undisturbed quantities. This work mainly focuses on seeking an accurate and efficient model to estimate the self-induced temperature perturbation and recover the undisturbed relative temperature for the thermal point-particle model.

The EL governing equations are derived by applying a homogeneous Gaussian filter of the following form

$$G_*(\boldsymbol{\xi}_*) = \frac{1}{(2\pi)^{3/2}\sigma_*^3} \exp\left[-\frac{|\boldsymbol{\xi}_*|^2}{2\sigma_*^2}\right], \tag{5}$$

where the Gaussian parameter $\sigma_* = \delta_*/(2\sqrt{2\ln 2})$ is the standard deviation and δ_* is the Gaussian width. Using this Gaussian filter we can define the fluid volume fraction and volume weighted temperature as

$$\phi(\mathbf{x}_*) = \int \chi(\mathbf{y}_*)\, G_*(\mathbf{x}_* - \mathbf{y}_*)\, d\mathbf{y}_*\,, \tag{6}$$

$$\overline{T}_{v*}(\mathbf{x}_*) = \phi(\mathbf{x}_*)\overline{T}_*(\mathbf{x}_*) = \int \chi(\mathbf{y}_*) T_*(\mathbf{y}_*)\, G_*(\mathbf{x}_* - \mathbf{y}_*)\, d\mathbf{y}_*\,, \tag{7}$$

where $\chi(\mathbf{y}_*)$ is the indicator function and it is equal to 1 inside the fluid and zero inside the particle. Subscript v means volume weighted quantity. A similar definition applies for velocity (see [1] for additional details).

Applying the Guassian filter to the governing equations, the volume averaged mass, momentum and energy equations become

$$\frac{\partial \phi}{\partial t_*} + \nabla_* \cdot \overline{\mathbf{u}}_{v*} = 0\,, \tag{8}$$

$$\frac{\partial \overline{\mathbf{u}}_{v*}}{\partial t_*} + \nabla_* \cdot (\overline{\mathbf{u}}_{v*}\overline{\mathbf{u}}_{v*}) = \frac{d\mathbf{U}_*}{dt_*} - \frac{1}{\rho_*}\nabla_* \overline{p}_{v*} + \nu_* \nabla_*^2 \overline{\mathbf{u}}_{v*} + \nabla_* \cdot (\mathbf{R}_{c*} + \mathbf{R}_{v*}) + \mathcal{F}_*\,, \tag{9}$$

$$\frac{\partial \overline{T}_{v*}}{\partial t_*} + \nabla_* \cdot (\overline{\mathbf{u}}_{v*}\overline{T}_{v*}) = \alpha_* \nabla_*^2 \overline{T}_{v*} + \nabla_* \cdot (\mathbf{R}_{cT*} + \mathbf{R}_{vT*}) + Q_*\,. \tag{10}$$

The averaging process results in unclosed terms when applied to the nonlinear and diffusion terms. The closure process then results in the residual stress terms in the momentum equation and corresponding residual flux terms in the energy equation shown above, which can be expressed as

$$\mathbf{R}_{c*} = \phi\,\overline{\mathbf{u}_*\,\mathbf{u}_*} - \overline{\mathbf{u}}_{v*}\overline{\mathbf{u}}_{v*} \quad \text{and} \quad \mathbf{R}_{v*} = \frac{\nu_*}{2}\left[\phi\left(\overline{\nabla_*\mathbf{u}_*} + \overline{(\nabla_*\mathbf{u}_*)^{\mathrm{T}}}\right) - \left(\nabla_*\overline{\mathbf{u}}_{v*} + (\nabla_*\overline{\mathbf{u}}_{v*})^{\mathrm{T}}\right)\right] \tag{11}$$

$$\mathbf{R}_{cT*} = -\phi\,\overline{\mathbf{u}_*\,T_*} - \overline{\mathbf{u}}_{v*}\overline{T}_{v*} \quad \text{and} \quad \mathbf{R}_{vT*} = \alpha_*\left[\phi\,\overline{\nabla_* T_*} - \nabla_*\overline{T}_{v*}\right]\,, \tag{12}$$

where the superscript "T" indicates transpose. The force and thermal coupling terms are approximated as

$$\mathcal{F}_* \approx -\frac{1}{\rho_*} G_*(\mathbf{x}_*) \oint_{|\mathbf{y}|=d_*/2} (-p_*\mathbf{I} + \boldsymbol{\tau}_*)\cdot\mathbf{n}\; d\mathbf{y}_* = \frac{\mathbf{F}_*}{\rho_*} G_*\,, \tag{13}$$

$$Q_* \approx G_*(\mathbf{x}_*) \oint_{|\mathbf{y}|=d_*/2} \alpha_*(-\nabla_* T_*)\cdot\mathbf{n}\; d\mathbf{y}_* = \frac{Q_*}{\rho_* c_{p*}} G_*\,, \tag{14}$$

In the above we have assumed the value of the Gaussian filter evaluated around the surface of the particle to be nearly uniform. This assumption has allowed the Gaussian filter to be moved out of the integral. The error in this assumption depends on the width of the Gaussian compared to the particle diameter. In the above, $\mathbf{n}$ stands for the surface normal unit vector, $\mathbf{I}$ represents the isotropic identity tensor, $\boldsymbol{\tau}_*$ is the viscous stress tensor and c_{p*} is the specific heat capacity at constant pressure. The total hydrodynamic force and heat flux from the particle back to the fluid are represented as $\mathbf{F}_*$ and Q_*.

We now non-dimensionalize the above equations with σ_* as the length scale, α_*/σ_* as the velocity scale, T_{f*} as the temperature scale, and $\rho_* \nu_*^2/\sigma_*^2$ as the pressure scale. We also consider the Stokes limit of zero Reynolds number where the nonlinear terms can be neglected. In this limit the thermal equation decouples and can be expressed as

$$\frac{\partial \overline{T}_v'}{\partial t} = \nabla^2 \overline{T}_v' + Q\,G\,, \tag{15}$$

The non-dimensional heat flux is defined as $Q = Q_*/(\lambda_* T_{f*} \sigma_*)$, where λ_* is the thermal conductivity of fluid. Since far away from the isolated particle $\phi \to 1$, we have the condition $\overline{T}_v \to 1$. This has allowed us to define the perturbation temperature as $\overline{T}'_v = \overline{T}_v - 1$. Also note that the Gaussian has been non-dimensionalized and we have ignored the residual fluxes in the above.

2.1. Exact EL Solution for Oscillatory Particle Motion in the Stokes Limit

Consider the following oscillatory feedback heat flux applied with the Gaussian spreading around the particle center, expressed in non-dimensional terms as

$$Q(t) = Q_\omega e^{-\iota\omega t}\,, \tag{16}$$

where the non-dimensional frequency (or Strouhal number) is given in terms of dimensional frequency as $\omega = \omega_* \sigma_*^2/\alpha_*$. The thermal equation (15) can be easily solved in different ways for the oscillatory heat flux. Here we solve by taking three-dimensional Fourier transform in space, since this approach will be pursued in the limit of small Reynolds number in Appendix A. The following solution for the volume averaged perturbation temperature results in the frequency space

$$\hat{T}'_{v\omega}(\mathbf{k}) = \frac{1}{k^2 - \iota\omega}\,\frac{Q_\omega}{(2\pi)^{3/2}}\,\exp\left[-\frac{k^2}{2}\right], \tag{17}$$

where $\mathbf{k}$ is the wave-vector and its magnitude is $k = |\mathbf{k}|$. As can be expected, in the zero Reynolds number limit the thermal field is isotropic and it depends only on the magnitude of the wave-vector. The perturbation temperature at the origin in real space can then be obtained as

$$[T'_{v\omega}]_p = T'_{v\omega}(\mathbf{x} = 0) = \frac{Q_\omega}{(2\pi)^{3/2}}\left[1 - \sqrt{\pi}\left(\sqrt{-\frac{\iota\omega}{2}}\right)\exp\left(-\frac{\iota\omega}{2}\right)\mathrm{erfc}\left(\sqrt{-\frac{\iota\omega}{2}}\right)\right], \tag{18}$$

where $[\quad]_p$ is used to denote properties evaluated at the particle center. The asymptotic behavior of the above solution can be obtained for large and small Strohal numbers as

$$[T'_{v\omega}]_p = \frac{Q_\omega}{(2\pi)^{3/2}} I_{\mathrm{T}}(\omega) \quad \text{where} \quad I_{\mathrm{T}}(\omega) = \begin{cases} 1 + \dfrac{i-1}{2}\sqrt{\pi\omega} + O(\omega) & \text{for} \quad \omega \ll 1 \\ \dfrac{3}{\omega^2} + \dfrac{\iota}{\omega} + O(\omega^{-3}) & \text{for} \quad \omega \gg 1 \end{cases}. \tag{19}$$

A plot of the transfer function $I_{\mathrm{T}}(\omega)$ is shown in Figure 1. The real part corresponds to perturbation temperature that is in-phase with the Gaussian heat source, and this is the only contribution in the steady limit. The imaginary part corresponds to perturbation temperature that is 90 degrees out-of-phase with the Gaussian heat source. From the figure it can be seen that for $\omega \gg 1$ the importance of the in-phase contribution becomes smaller.

3. Numerical Methodology

The analytical solution of the previous section applies only in the Stokes limit. We turn to numerical simulations for answers at finite Re_σ. Here it is far more convenient to non-dimensionalize in terms of inertial scaling. We choose σ_* as the length scale, and $U_* = |\mathbf{U}_*|$ as the velocity scale, T_{f*} as the temperature scale, $\rho_* U_*^2$ as the pressure scale and $\rho_* U_*^2 \sigma_*^2$ as the force scale. All these inertially scaled non-dimensional variables are denoted with a tilde and we define $\tilde{Q} = Q_*/(\rho_* c_{p*} U_* T_{f*} \sigma_*^2)$.

The resulting non-dimensional governing equations are solved numerically in a large enough cuboidal

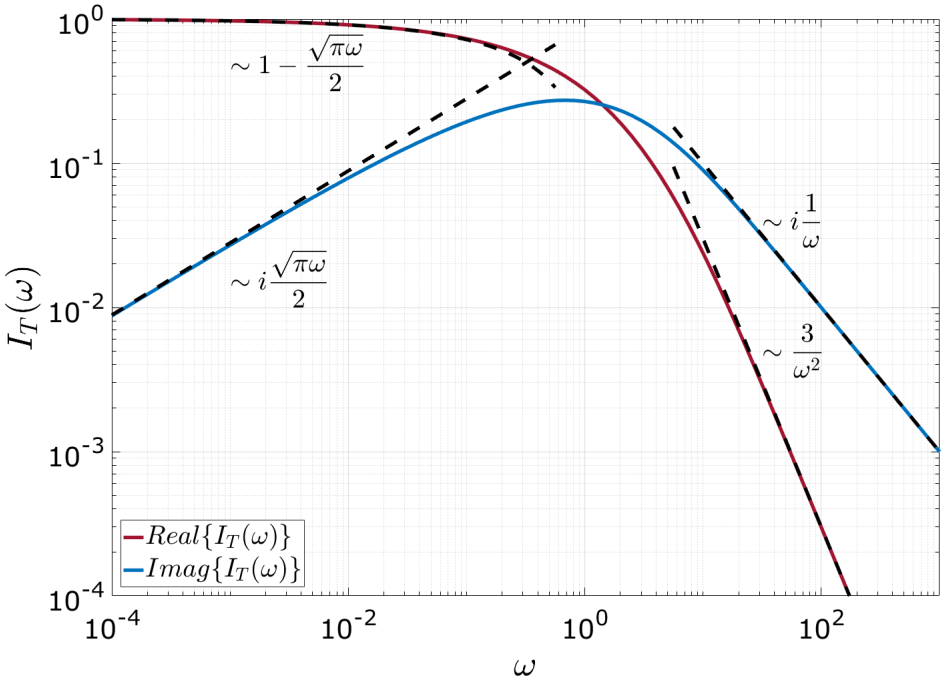

Fig. 1: Plot of $I_T(\omega)$ along with the asymptotic solutions of equation (19).

domain of size $[-20, 20]$, $[-24, 40]$ and $[-20, 20]$, along the (x, y, z) directions, where the flow is chosen to be in the positive y-direction in the frame attached to the particle. In this frame, the feedback force and heat transfer to the fluid are applied as Gaussian filtered $\tilde{\mathbf{F}}\tilde{G}$ and $\tilde{Q}\tilde{G}$ centered around the origin. A steady unit far-field velocity is applied in the y-direction at both the inflow and on the side boundaries of the domain. At the top surface a buffer region is applied as the outlet boundary condition, since the Gaussian wake region is long.

The simulations were performed using the spectral element code Nek5000 [22], in which the whole domain is split into $5 \times 8 \times 5$ cubic elements. Three-dimensional Gauss-Lobatto-Legendre grids are generated within each element and the polynomial order used here is 16. Therefore, the non-dimensional average grid size is $\widetilde{\Delta x} = 0.5$. Since σ_* is the length scale, the non-dimensional Gaussian width is $\tilde{\delta} = 2\sqrt{2\ln 2} \approx 2.355$. The Prandtl number is chosen as unity in all the simulations. The key physical parameters of the simulation are Pe_σ, $\tilde{F}$ and $\tilde{Q}$. The only other numerical parameter of relevance is the ratio $\delta_*/\Delta x_*$, which measures the number of grid points resolving the Gaussian width. Here this ratio has been chosen to be 4.71. It was observed in [1] that the self-induced velocity correction results are insensitive to the precise value of this numerical parameter, and this observation equally applies in the present case of thermal correction as well.

Two example numerical thermal fields are displayed in Figure 2 for two different values of Peclet number. Only part of the computational domain close to the particle is shown. From the figure it is clear that the spherically symmetric perturbation of the zero Peclet number develops a front-back asymmetry at finite Peclet number and this asymmetry increases with increasing Re_σ. As pointed

out in [1] the flow at the higher Peclet number corresponds to a jet-like flow from an intense point momentum source and the corresponding thermal field of the jet-like flow is seen in frame (b). In the lower Peclet number case the wake is much smaller and contained within the immediate neighborhood of the particle [23].

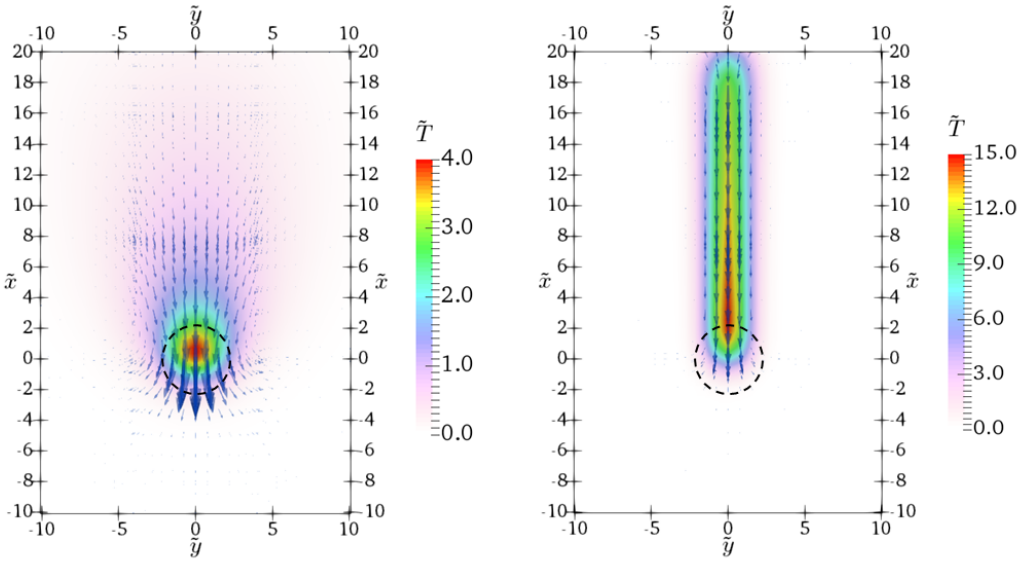

Fig. 2: Contours of fluid temperature $\tilde{T}$ and perturbation velocity vectors plot on the $X-Y$ plane passing through the center of the particle for the two cases of (a) $\mathrm{Pe}_\sigma = 1$ and (b) $\mathrm{Pe}_\sigma = 100$. The black dashed circle indicates the Gaussian filter half width $\delta = 2.355$ (which corresponds to $\sigma = 1$). In both cases the feedback force magnitude is $\tilde{F} = 3.5 \times 10^{-2}$ and the interphase heat flux is $\tilde{Q} = 100$.

4. Quasi-steady temperature correction

First, we study the self-induced temperature perturbation in the quasi-steady limit, where the history effect is not important. The analytical solution of the Stokes limit will be used along with empirical extension to finite Peclet number based on results from numerical simulations. In the analytical expression (19) of the previous section we substitute $I(\omega \to 0) \to 1$, and convert the solution to dimensional variables and obtain the result

$$\left[\overline{T}'_*\right]_p = \frac{Q_*}{(2\pi)^{3/2}\sigma_*\lambda_*\phi_0} + \left(\frac{1}{\phi_0} - 1\right) T_{f*}\,, \tag{20}$$

where Q_* is the feedback heat source. Here ϕ_0 is the fluid volume fraction at the particle center, which can be expressed as (see [18, 1])

$$\phi_0 = 1 - \mathrm{erf}\left[\frac{d_*}{2\sqrt{2}\sigma_*}\right] + \sqrt{\frac{1}{2\pi}}\frac{d_*}{\sigma_*}\exp\left[-\frac{d_*^2}{8\sigma_*^2}\right]. \tag{21}$$

The second term on the right in (20) is simply due to the fact that part of the averaging volume is occupied by the particle whose temperature is different from that of the fluid. This contribution remains non-zero even when there is no thermal feedback from the particle. However, this perturbation

is typically much smaller than that due to thermal feedback, which is represented by the first term on the right. The division by ϕ_0 on the right hand side arises from the undoing of the volume fraction weighting.

Note that the present work assumes the flow to be decoupled from the thermal field. This is appropriate only in the limit of externally driven flows where the temperature-induced density variation within the fluid and any resulting buoyancy-induced flow is not of importance. Within this approximation, however, no further assumption has been made about the nature of heat transfer. As a result the above result is independent of the specific form of heat transfer correlation and therefore applies to rigid particles, droplets and bubbles. Now we specialize the analysis by assuming the heat transfer to be given by the standard thermal point-particle model in the Stokes limit for a rigid spherical particle: $Q_* = -2\pi\lambda_* d_* T_{f*}$, where d_* is the particle diameter. By substituting this back into the self-induced temperature perturbation equation (20), the disturbed particle center temperature becomes

$$\left[\overline{T}_*\right]_p = \frac{T_{f*}}{\phi_0}\left(1 - \frac{1}{\sqrt{2\pi}}\frac{d_*}{\sigma_*}\right). \tag{22}$$

Note that according to the above quasi-steady model, if the perturbed temperature in an EL simulation slowly varies with time as $\left[\overline{T}_*\right]_p(t_*)$ the corresponding true undisturbed fluid temperature $T_{f*}(t_*)$ must also be slowly varying, and can be calculated as given in the above equation. Figure 3 shows the variation of $1 - d_*/(\sqrt{2\pi}\sigma_*)$, ϕ_0 and their ratio as a function of δ_*/d_* or σ_*/d_*. It can be seen in the plot that the non-dimensional particle center temperature increasingly deviates from the true undisturbed value of unity for a narrower Gaussian filter. This is because the heat source/sink fed back to the fluid is more concentrated near the particle center and causes substantial perturbation. For sufficiently concentrated feedback, the disturbed particle center temperature can even change sign and result in more than 100% error in point-particle temperature. On the other hand, for larger Gaussian width, i.e., for $\sigma_*/d_* \gg 1$ the self-induced perturbation temperature becomes small. Even at $\sigma_*/d_* = 2$ the error is 25%. Fortunately this large error is limited to the Stokes regime and rapidly decreases with increasing Reynolds/Peclet number. Over the entire range of σ_*/d_*, the effect of volume fraction correction represented by the factor ϕ_0 is quite small (see [18, 1]).

4.1. Correction at finite Peclet number

Now we extend the quasi-steady self-induced temperature from Stokes limit to finite Peclet number. Here Peclet number is defined as

$$\mathrm{Pe}_\sigma = \frac{\sigma_* U_*}{\alpha_*} = \mathrm{Re}_\sigma\ \mathrm{Pr}\,, \tag{23}$$

where the Reynolds number based on the Gaussian width is $\mathrm{Re}_\sigma = \sigma_* U_*/\nu_*$ and the Prandtl number $\mathrm{Pr} = \nu_*/\alpha_*$. Note that the above Peclet number is defined based on the Gaussian function as the length scale. It can be related to the standard Peclet number based on particle diameter through the relation $\mathrm{Pe}_\sigma = \mathrm{Pe}(\sigma_*/d_*)$. The analytical derivation using the Oseen's approximation is presented in Appendix A. Although the resulting expression is only accurate for very small Pe_σ, its functional form is used to obtain an empirical correction that is valid over a wider range of Peclet number using the numerical simulation results. This correction term is fitted for a range of Peclet number Pe_σ and non-dimensional feedback force magnitude $\tilde{F} = \left|\tilde{\mathbf{F}}\right|$.

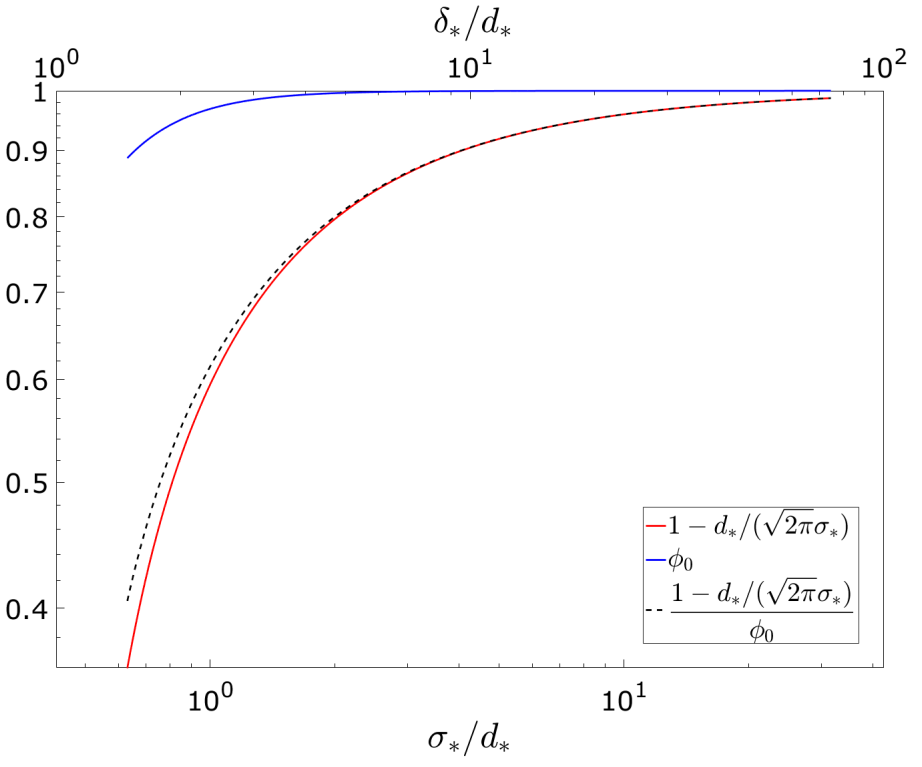

Fig. 3: Plot of $1 - \frac{1}{\sqrt{2\pi}}\frac{d_*}{\sigma_*}$, ϕ_0 and their ratio extracted from the self-induced temperature equation (22).

According to Appendix A, the self-induced temperature perturbation at the particle center can be written as

$$\left[\overline{T}'_*\right]_p = \frac{Q_*}{(2\pi)^{3/2}\sigma_*\lambda_*\phi_0}\Psi_{\mathrm{T}}\left(\mathrm{Pe}_\sigma, \tilde{F}\right) + \left(\frac{1}{\phi_0} - 1\right)T_{f*}\,. \tag{24}$$

Due to the linearity of the energy equation in temperature, the self-induced perturbation scales linearly with the feedback heat source. The nonlinear effect arises only from the momentum equation through the parameters Pe_σ and $\tilde{F}$. The fluid volume fraction at the particle location ϕ_0 is generally very close to unity (see Figure 3) and as a result the second term on the right is much smaller and can be ignored. $\Psi_{\mathrm{T}}\left(\mathrm{Pe}_\sigma, \tilde{F}\right)$ accounts for the non-linear effect of finite Peclet number and the convective heat transfer induced by the feedback force. This term can be written as its Oseen's approximation obtained in the Appendix multiplied by a correction function as

$$\Psi_{\mathrm{T}}\left(\mathrm{Pe}_\sigma, \tilde{F}\right) = \Psi_{\mathrm{Tos}}\left(\mathrm{Pe}_\sigma\right)\chi_T\left(\mathrm{Pe}_\sigma, \tilde{F}\right)\,. \tag{25}$$

In order to obtain a functional fit for χ_T, we performed 162 simulations in total by choosing 9 different values of Peclet numbers $\mathrm{Pe}_\sigma = \left[10^0, 10^{0.5}, 10^1, 10^{1.5}, 10^2, 10^{2.5}, 10^3, 10^{3.5}, 10^4\right]$, 6 different values of feedback force magnitudes $\tilde{F} = [0.0035, 0.035, 0.35, 0.7, 1.73, 3.5]$ and 3 different values of the grid resolution $\delta_*/\Delta x_* = [2, 4, 8]$. The feedback force is always directed opposite to the far-field ambient flow velocity $\mathbf{U}_*$. Note that δ_* is related to σ_* through the relation $\delta_* = 2\sqrt{2\ln 2}\sigma_*$. Since δ_* has the clear interpretation as the Gaussian width, its resolution in terms of $\delta_*/\Delta x_*$ is presented.

Results show that $\delta_*/\Delta x_* = 4$ is fine enough to get converged results that are identical to those with $\delta_*/\Delta x_* = 8$, while $\delta_*/\Delta x_* = 2$ is not adequate and gives results that deviate slightly from the finer resolution results. These observations are similar to those reported in [1] and will not be repeated. Further discussions are based on $\delta_*/\Delta x_* = 4.71$ simulations.

We assume the following functional form for the correction χ_T

$$\chi_T\left(\mathrm{Pe}_\sigma, \tilde{F}\right) = 10^{\left[A(\mathrm{Pe}_\sigma)\tilde{F} + B(\mathrm{Pe}_\sigma)\tilde{F}^2\right]}, \tag{26}$$

and the numerical simulation results are used to obtain the following expressions for the two coefficients

$$A(\mathrm{Pe}_\sigma) = 0.022 \exp\left[-2.425\, \mathrm{Pe}_\sigma^{-1.053}\right],$$
$$B(\mathrm{Pe}_\sigma) = 0.0021 \exp\left[-6.578\, \mathrm{Pe}_\sigma^{-1.068}\right]. \tag{27}$$

Figure 4a shows a plot of Ψ_T as a function of Pe_σ obtained from the numerical simulation results along with the analytical expression Ψ_{Tos}. As can be seen the difference is small on the logarithmic scale. The Oseen's prediction is quite good (i) for small values of $\tilde{F}$ for all Peclet number and (ii) for small Peclet number for all values of $\tilde{F}$. Only for large Pe_σ and large $\tilde{F}$ the departure from Oseen's result is significant. This is illustrated in Figure 4b in the plot of the correction function χ_T, which departs from 1.0 only for large values of Pe_σ and $\tilde{F}$. It can be observed that the numerical results are well approximated by the curve fit given above.

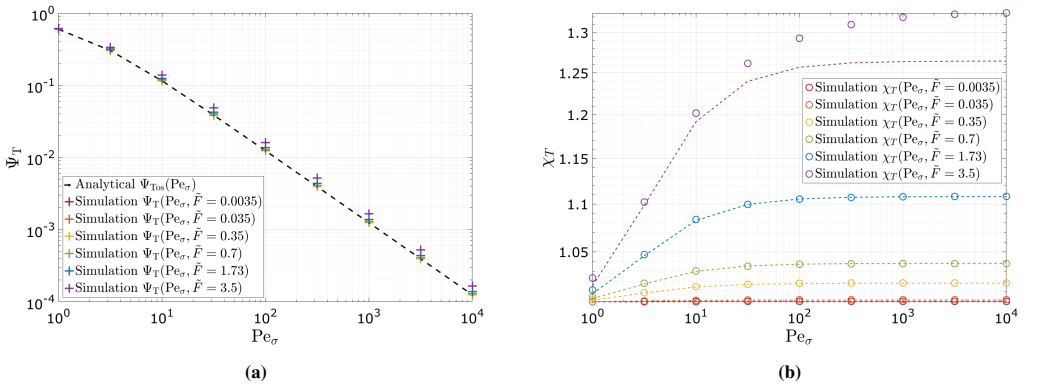

Fig. 4: (a) Component of self-induced temperature perturbation. (b) Correction factor for finite Pe_σ. The dashed lines are the fitted function 26.

We now compare the present results for self-induced thermal correction with the results obtained in [1] for self-induced velocity correction. Figure 5a compares the Ψ_{Tos} obtained in the present thermal problem with that for the velocity. For large values of Re_σ their ratio reaches the largest value of $3/2$. This agreement in their behavior is not surprising since it is indeed the nonlinear advection that controls both the velocity and thermal perturbations. It should however be noted that while Ψ_{os} for velocity is plotted as a function of Re_σ, the function Ψ_{Tos} for temperature is plotted as a function of Pe_σ. Thus, for $\mathrm{Pr} \ll 1$, the thermal correction will be far more important since $\mathrm{Pe}_\sigma \ll \mathrm{Re}_\sigma$, while the converse is true for fluids of large Prandtl number. Figure 5b compares the functional dependence of

χ_T for the thermal problem against the corresponding corrections for the velocity problem. It can be seen that in both cases the correction factor χ approaches unity as $\tilde{F}$ becomes small (for $\tilde{F} = 0.035$ and 0.0035 the curves are visually indistinguishable). Again the behaviors are quire similar even quantitatively for the entire range of $\tilde{F}$ values considered.

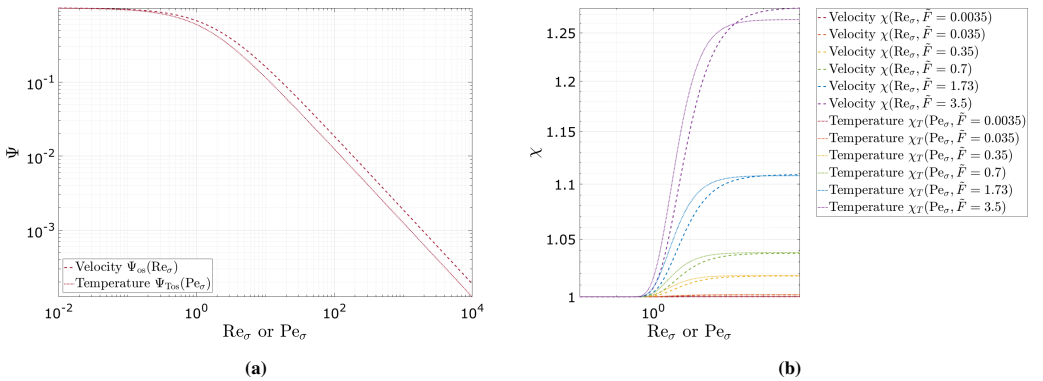

(a) **(b)**

Fig. 5: (a) Component comparison between self-induced velocity and temperature in the Stokes limit. (b) Comparison of the correction factor between self-induced velocity and temperature in the Stokes limit. In both figures the Prandtl number is 1.

5. Unsteady temperature correction

The results of the steady-state analysis is sufficient as long as the time rate of change of feedback heating of the fluid is not strong. In this case the steady-state results can be applied at each instant of the slowly varying problem and hence we call this approach "quasi-steady correction". In many situations the time rate of change of feedback heating is not small. Even if the feedback heating were to slowly vary, the feedback force or the Reynolds number can undergo rapid variation, which will invalidate the quasi-steady assumption in both the velocity and thermal correction models. In these situations, one must consider the unsteady problem and develop an appropriate model of the self-induced thermal correction. Again, we first derive an analytical expression for the unsteady self-induced thermal perturbation in the Stokes limit, and then extend it to the finite Peclet number regime using the results of numerical simulations performed under controlled unsteady conditions.

5.1. Correction in the Stokes limit

Starting from the analytical expression (18) for the self-induced temperature perturbation in the frequency domain, following the steps outlined in [1], we can obtain the following time domain result

$$\left[\overline{T}'_*\right]_p(t_*) = \frac{1}{(2\pi)^{3/2}\sigma_*\lambda_*\phi_0}\left[Q_*(t_*) - \int_{-\infty}^{t_*} K_{T0}(t_* - \tau_*)\left.\frac{dQ_*}{dt_*}\right|_{\tau_*} d\tau_*\right] + \left(\frac{1}{\phi_0} - 1\right)T_{f*}\,, \tag{28}$$

where K_{T0} is the zero-Reynolds number unsteady thermal kernel given by

$$K_{T0}(t_* - \tau_*) = \frac{1}{\sqrt{1 + \dfrac{2\alpha_*(t_* - \tau_*)}{\sigma_*^2}}}\,, \tag{29}$$

5.2. Correction at finite Peclet number

In the finite Peclet number case, two changes can be naturally expected. First, the non-linear term from the quasi-steady model should be added here to account for the Reynolds number effect on slow variation. Second, the unsteady-diffusive kernel should be improved to account for its dependence on Peclet number. Ignoring the small volume fraction contribution of the second term on the right hand side of (28), the unsteady volume-weighted self-induced temperature model can be written as (because of volume weighting we now have the added subscript v in $\left[\overline{T}'_{v*}\right]_p$ and ϕ_0 has been removed from the denominator)

$$\left[\overline{T}'_{v*}\right]_p(t_*) = \frac{1}{(2\pi)^{3/2}\sigma_*\lambda_*}\left\{Q_*(t_*)\Psi_{\mathrm{T}}\left(\mathrm{Pe}_\sigma,\tilde{F}\right) - \int_{-\infty}^{t_*} K_T(t_*-\tau_*;\mathrm{Pe}_\sigma)\left.\frac{d\left[Q_*\Psi_{\mathrm{T}}\left(\mathrm{Pe}_\sigma,\tilde{F}\right)\right]}{dt_*}\right|_{\tau_*} d\tau_*\right\}, \tag{30}$$

where $\Psi_{\mathrm{T}}\left(\mathrm{Pe}_\sigma,\tilde{F}\right)$ was introduced in (25). The kernel $K_T(t_*-\tau_*;\mathrm{Pe}_\sigma)$ must however be empirically recovered from the results of appropriately constructed numerical simulations in the unsteady regime. One approach is to consider response to a step jump in the heat flux and use the resulting temperature time history at the particle location to obtain the kernel. Specifically, assume the velocity and temperature fields have already reached steady state, then we suddenly increase the heat flux from $\tilde{Q}_0$ to $\tilde{Q}_1$ instantly at time $\tilde{t}_1$. Another option to introduce time-dependence is to suddenly change the feedback force. Both these changes can be applied simultaneously as well. Irrespective of the precise nature of the sudden change, its effect will manifest as rapid variation in self-induced temperature and according to the unsteady thermal correction model presented above in (30), the volume-weighted self-induced temperature perturbation is expected to follow

$$\left[\tilde{T}'_v\right]_p(\tilde{t}) = \begin{cases} \dfrac{\tilde{Q}_0\,\mathrm{Pe}_\sigma\,\Psi_{\mathrm{T}}\left(\mathrm{Pe}_\sigma,\tilde{F}_0\right)}{(2\pi)^{3/2}} & \text{for} \quad \tilde{t}\leqslant\tilde{t}_1 \\ \dfrac{\tilde{Q}_1\,\mathrm{Pe}_\sigma\,\Psi_{\mathrm{T}}\left(\mathrm{Pe}_\sigma,\tilde{F}_1\right) - K_T\left(\tilde{t}-\tilde{t}_1;\mathrm{Pe}_\sigma\right)\left[\tilde{Q}_1\,\mathrm{Pe}_\sigma\,\Psi_{\mathrm{T}}\left(\mathrm{Pe}_\sigma,\tilde{F}_1\right) - \tilde{Q}_0\,\mathrm{Pe}_\sigma\,\Psi_{\mathrm{T}}\left(\mathrm{Pe}_\sigma,\tilde{F}_0\right)\right]}{(2\pi)^{3/2}} & \text{for} \quad \tilde{t}>\tilde{t}_1\,, \end{cases} \tag{31}$$

where $\tilde{F}_1$ is the feedback force after the step change. After some algebraic manipulation the finite Peclet number kernel can then be extracted by rewriting the above expression as

$$\begin{aligned} K_T(\tilde{\xi};\mathrm{Pe}_\sigma) &= \frac{\tilde{Q}_1\,\mathrm{Pe}_\sigma\,\Psi_{\mathrm{T}}\left(\mathrm{Pe}_\sigma,\tilde{F}_1\right) - (2\pi)^{3/2}\left[\tilde{T}'_v\right]_p(\tilde{t}_1+\tilde{\xi})}{\tilde{Q}_1\,\mathrm{Pe}_\sigma\,\Psi_{\mathrm{T}}\left(\mathrm{Pe}_\sigma,\tilde{F}_1\right) - \tilde{Q}_0\,\mathrm{Pe}_\sigma\,\Psi_{\mathrm{T}}\left(\mathrm{Pe}_\sigma,\tilde{F}_0\right)} \\ &= \frac{\left[\tilde{T}'_v\right]_p(\tilde{t}\to\infty) - \left[\tilde{T}'_v\right]_p(\tilde{t}_1+\tilde{\xi})}{\left[\tilde{T}'_v\right]_p(\tilde{t}\to\infty) - \left[\tilde{T}'_v\right]_p(\tilde{t}_1)} \quad \text{for} \quad \tilde{\xi}\geqslant 0\,, \end{aligned} \tag{32}$$

where $\tilde{\xi}=\tilde{t}-\tilde{t}_1$ is the elapsed time from the instant of jump in the heat flux. The final expression is entirely in terms of the time history of the perturbed temperature and has been appropriately normalized. $\left[\tilde{T}'_v\right]_p(\tilde{t}_1)$ is the perturbed temperature at the particle prior to the jump in heat flux (or the old steady state temperature corresponding to $\tilde{Q}_0$ and $\tilde{F}_0$), while $\left[\tilde{T}'_v\right]_p(\tilde{t}\to\infty)$ is the new steady state temperature that results from the new heat flux $\tilde{Q}_1$ and $\tilde{F}_1$.

The numerical results indicate that the effect of feedback force magnitude on the thermal history kernel can be ignored. The kernel obtained for cases that range from $\tilde{F}=0.0035$ to $\tilde{F}=3.5$ yielded almost the same result. The numerically extracted history kernel shows two asymptotic behaviors:

(i) For the short time, the history kernel follows the analytical form (29) obtained in the Stokes limit, which is a function of time $\xi = \xi_* \alpha_* / \sigma_*^2$ that has been non-dimensionalized using viscous scale. This scaling is appropriate at small time, because diffusive heat transfer is the dominant mechanism during the early history. (ii) For the long-time evolution, the history kernel follows a much faster exponential decay and the kernels collapse when expressed as a function of $\tilde{\xi} = \xi_* U_* / \sigma_*$ that has been non-dimensionalized with inertial scales (due to the dominance of the nonlinear effect over long-time). These asymptotic solutions are expressed as follows

$$K_T(\tilde{\xi}; \mathrm{Pe}_\sigma) = \begin{cases} \dfrac{1}{\sqrt{1 + 2\,\tilde{\xi}/\,\mathrm{Pe}_\sigma}} & \text{for} \quad \tilde{\xi} \ll 1 \\ \exp\left(-2.356\,\tilde{\xi}\right) & \text{for} \quad \tilde{\xi} \gg 1 \end{cases} . \tag{33}$$

It should be noted that the long-term exponential decay was observed in the case of unsteady self-induced velocity correction as well [1]. The transition time at which the change from early one-over-square-root decay to the late time exponential decay occurs depends on the Peclect number. For small Peclet number, as can be expected, the agreement with the analytical kernel (29) persists for longer time and the approach to exponential decay is delayed. Whereas, with increasing Peclet number the agreement with the analytical kernel (29) is only for a very brief early period and the kernel soon starts to decay exponentially. In this paper, we use the complementary error function $f(\tilde{\xi}) = \mathrm{erfc}\left[c_1\left(c_2^{\tilde{\xi}} - c_3\right)\right]$ to blend the two asymptotic answers together. The fitted values of the three coefficients of the function at different Pe_σ are shown in Table 1. One can obtain the coefficients for intermediate values of Pe_σ, not listed in the table, through interpolation. Then the composite history kernel can be expressed as

$$K_T(\tilde{\xi}; \mathrm{Pe}_\sigma) = f(\tilde{\xi})\,\frac{1}{\sqrt{1 + 2\,\tilde{\xi}/\,\mathrm{Pe}_\sigma}} + [1 - f(\tilde{\xi})]\exp\left(-2.356\,\tilde{\xi}\right) . \tag{34}$$

The slow to fast decay of the above kernel and its dependence on Peclect number is similar to the behavior observed for velocity correction kernel and is also similar to the finite Reynolds number correction to the Basset history kernel.[241992Mei and Adrian] In the limit $\tilde{\xi} \to 0$ both the terms on the right approach unity and the precise value of f in this limit is not very important. Thus, the complementary error function fit for $f(\tilde{\xi})$ has been tailored to capture the long-time decay.

Figure 6 shows the kernel extracted from the numerical simulations compared to the empirical fit presented above. Excellent agreement between the empirical fits and the numerical results at both early and late times can be seen in the log-scale and linear-scale plots. Also shown in the plot is the zero Peclet number analytical kernel. When plotted in terms of the viscous time scale, all the kernels start from the analytical behavior (29) when $\xi \ll 1$, but finally evolve into exponential decay with the same decay rate. This transition happens earlier for larger Pe_σ. Instead, if plotted in terms of inertially scaled time $\tilde{\xi}$ all the kernels collapse in their exponential decay at sufficiently late time. For very large Pe_σ the exponential decay is early and fast, and therefore the kernel is virtually zero and can be ignored. In other words, in the limit of very large Peclet number the problem can be considered essentially quasi-steady. At lower Peclet numbers the unsteady model may be necessary if the ambient flow conditions vary sufficiently rapidly.

6. Testing of the Steady & Unsteady Models

In this section, we evaluate the accuracy of the self-induced temperature correction model when it is implemented in the two-way coupled Euler-Lagrange simulation. The test setup will be simple and it will cover a range of parameter values of interest. Though the simplified test conditions

Table 1: Fitted parameters in the blending function for different Pe_σ.

Pe_σ	c_1	c_2	c_3
1	28.6521	1.0052	0.9869
$\sqrt{10}$	27.7924	1.0111	0.9880
10	8.92552	1.0506	0.9669
$10\sqrt{10}$	3.32093	1.1526	0.9123
100	2.55624	1.2051	0.8857
$100\sqrt{10}$	2.15369	1.2434	0.8617
1000	2.09725	1.2507	0.8579
$1000\sqrt{10}$	2.04844	1.2566	0.8542
10000	2.02633	1.2592	0.8525

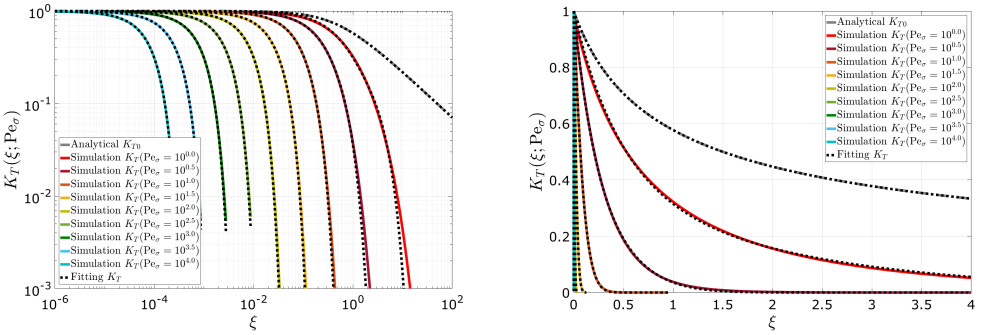

Fig. 6: Plot of the history kernel with respect to the viscous non-dimensional time (a) log scale and (b) linear scale. The analytical solution K_{T0} in the Stokes limit is represented by the black dashed line and the fitted kernel (34) is the black dotted lines. 9 different kernels from simulations with different Pe_σ are shown. The kernels are independent of the feedback force.

are synthetic, the conclusions to be drawn are of relevance to wide range of practical conditions. Given an isolated particle in an undisturbed uniform ambient flow of constant velocity $\mathbf{U}_*$ (magnitude $U_* = |\mathbf{U}_*|$) and uniform temperature T_{0*}, we consider convective heat transfer to the particle when the ambient temperature is varied exponentially to its terminal value. The particle is held static in position and the feedback force $\mathbf{F}_*$ is applied to the surrounding fluid with a Gaussian filter of standard deviation σ_*. We have considered different non-dimensional values of the feedback force $\tilde{F} = |\mathbf{F}_*|/(\rho_* U_*^2 \sigma_*^2)$, but here we only discuss results from $\tilde{F} = 1.73$, since the results to be presented are insensitive to the value of $\tilde{F}$. The particle is assumed to be isothermal and maintained at the constant temperature of the initial ambient fluid $\tilde{T}_0$ at all time. In the test cases, as the undisturbed ambient temperature increases exponentially we correspondingly increase the heat flux to the particle exponentially as given in the following expressions

$$\tilde{T}(t) = \tilde{T}_0 + \Delta\tilde{T}\left[1 - \exp(-\tilde{t}/\tilde{\tau}_\theta)\right], \tag{35}$$

$$\tilde{Q}(t) = \Delta\tilde{Q}\left[1 - \exp(-\tilde{t}/\tilde{\tau}_\theta)\right], \tag{36}$$

where $\tilde{\tau}_\theta$ is the time scale of temperature variation, which dictates how fast the undisturbed temperature is varied. The temperature of the particle is held fixed during the entire period. Therefore, $\tilde{T}_0 + \Delta\tilde{T}$, and $\Delta\tilde{Q}$ are the terminal values of ambient temperature and the heat flux due to the temperature difference. We report results from 9 numerical simulations with different values of Peclet number $\mathrm{Pe}_\sigma = [1, \sqrt{10}, 10]$ and non-dimensional time scale of thermal variation $\tilde{\tau}_\theta = \tau_{\theta*} U_*/\sigma_* = [0.1, 1, 10]$. The non-dimensional heat flux has been set to $\Delta\tilde{Q} = \Delta Q_*/(\rho_* c_{p*} U_* T_{0*} \sigma_*^2) = -10$ and the results to be presented are linear in this quantity. In all these simulations we assume the fluid volume fraction is 1 everywhere since σ_*/d_* is constant and large enough and we record the time history of fluid temperature at particle center, which is the disturbed fluid temperature.

From the quasi-steady and unsteady models we predict the disturbed temperature at the particle center by superposing the model prediction of self-induced temperature perturbation to the undisturbed ambient temperature (see equation (4)). The self-induced temperature is computed using the quasi-steady (24) and unsteady (30) correction models, respectively, at every simulation time step. The prediction accuracy of the models are then evaluated by comparing with the corresponding numerical simulation results. The temperature evolution curves for $\mathrm{Pe}_\sigma = 1, 10$ and $\tilde{\tau}_\theta = 0.1, 1, 10$ are shown in Figure 7.

The black dashed line is the imposed exponentially increasing undisturbed ambient fluid temperature and the blue dashed line is the computed disturbed fluid temperature at the center of the particle. The gap between the black and blue lines is the self-induced temperature perturbation $\left[\tilde{T}'\right]_p$ as computed in the simulation. The terminal value of $\left[\tilde{T}'\right]_p$ is independent of $\tilde{\tau}_\theta$ and it increases with Pe_σ. This is because the larger Pe_σ means smaller thermal diffusivity, which results in stronger local temperature disturbance. This behavior is consistent with the result of the self-induced velocity, which also increases with Re_σ.

When the temperature of the undisturbed flow was increased very rapidly above the initial temperature (i.e., for small values of $\tilde{\tau}_\theta$) the filtered temperature at the origin also rapidly increases and the effect of the particle's temperature remaining at the lower initial value is perceived by the fluid in a delayed manner. This results in an initial slow growth in $\left[\tilde{T}'\right]_p$ (which is the difference between the undisturbed temperature and the DNS temperature at the particle center), followed by a faster growth towards the terminal value. With increasing $\tilde{\tau}_\theta$ the ambient temperature increases to the terminal value slowly enough that $\left[\tilde{T}'\right]_p$ approaches its terminal value in a uniform way. This behavior is well captured by the unsteady model and thus with the unsteady model, the perturbed fluid temperature evaluated at the center of the particle in an EL simulation can be reliably corrected to obtain the corresponding true undisturbed ambient fluid temperature. In contrast, the quasi-steady correction model approaches the terminal state monotonically. The speed of this approach is exactly the same as that imposed by the variation of the undisturbed ambient temperature. Thus, the quasi-steady correction model overestimates the self-induced temperature correction, and this overestimation increases as the time scale of variation decreases. Figure 8 shows the maximum absolute error of self-induced temperature perturbation in each of the 9 cases.

The above results are in terms of Pe_σ and $\tilde{\tau}_\theta$, both of which are defined in terms of the numerical length scale σ_* of the EL methodology. We now relate the above results to physical and more familiar parameters such as particle Peclet number, $\mathrm{Pe} = d_* U_*/\alpha_*$ and particle thermal Stokes number $\mathrm{St}_{th} = d_* U_* \rho\, C_r/(12\alpha_*)$, where ρ is particle-to-fluid density ratio and C_r particle-to-fluid specific heat ratio. First, we note that $\mathrm{Pe} = \mathrm{Pe}_\sigma(d_*/\sigma_*)$ and thus the particle Peclet number is typically smaller

than Pe_σ. For any given physical problem of known Pe, its numerical implementation will dictate the correspondingPe$_\sigma$ through the choice of nondimensional ratio d_*/σ_*.

Though the test problem considered a particle of constant temperature in a time-varying thermal evolution of the ambient fluid, the results equally apply for a particle undergoing unsteady thermal evolution in a steady thermal ambient. Thus $\tau_{\theta *}$ can also be interpreted as the particle thermal time scale, or the time scale on which a particle exposed to a constant ambinet temperature will evolve. The thermal Stokes number of the particle $\mathrm{St}_{th} = \tau_{\theta *} U_*/d_* = \tilde{\tau}_\theta \sigma_*/d_*$. Thus, St_{th} is typically larger than the numerical parameter $\tilde{\tau}_\theta$ used in the test.

7. Discussion

In this section we answer the following two questions: (i) under what condition a thermal correction is warranted and (ii) if a thermal correction is needed, under what condition the more complex unsteady correction is warranted. We seek precise answer to both these questions that can be formulated into simple criterion that can be implemented easily. The answer to both these questions will however depend on the desired level of accuracy. A stringent criterion may require 1% accuracy, while a relaxed criterion applies if a higher level of error can be tolerated.

We define β to be the acceptable level of relative temperature perturbation, which is defined as the ratio of self-induced temperature perturbation versus the difference in temperature between the particle and the undisturbed ambient fluid. If the relative temperature perturbation is larger than β, then either the quasi-steady or unsteady correction model for self-induced temperature should be adopted in the two-way coupled Euler-Lagrange simulation. Otherwise, the EL simulation can proceed without correcting the fluid temperature evaluated at the particle center. Since the self-induced temperature perturbation depends primarily on non-dimensional heat flux $\tilde{Q} = Q_*/(\rho_* c_{p*} U_* T_{f*} \sigma_*^2)$ and Pe_σ, we can establish a critical heat flux function $\tilde{Q}_{\mathrm{cr}}(\beta, \mathrm{Pe}_\sigma)$, and for a given Peclet number if the actual heat flux $\tilde{Q}$ exceeds the critical value then thermal correction is required.

From Figure 7 we note that the predicted thermal perturbation of the quasi-steady model is larger than the unsteady model. Therefore, a conservative estimate of $\tilde{Q}_{\mathrm{cr}}$ can be obtained with the quasi-steady thermal correction model as

$$\tilde{Q}_{\mathrm{cr}} = \frac{4\pi\beta}{1 - \exp\left(\dfrac{\mathrm{Pe}_\sigma^2}{2}\right) \cdot \mathrm{erfc}\left(\dfrac{\mathrm{Pe}_\sigma}{\sqrt{2}}\right)}. \tag{37}$$

Then, the criterion for correction will be that when the non-dimensional heat flux $\tilde{Q}$ is larger than the critical value $\tilde{Q}_{cr}$ correction is needed. This criterion makes the following two simplifications: (i)The Gaussian filter width δ_* is larger than the particle diameter d_*, so the volume fraction effect is ignored. (ii) The finite Peclet number and the finite feedback force effects that appear through the correction χ_T are neglected, since they are generally close to unity.

Specifically, in a two-way coupled Euler-Lagrange simulation, if the particle-to-fluid heat flux $\tilde{Q} > \tilde{Q}_{cr}$, the self-induced temperature correction is required to guarantee that the undisturbed ambient fluid temperature can be accurately calculated from the temperature of the EL simulation interpolated to the particle center. Only then the heat flux can be accurately calculated with the point-particle heat transfer model. In cases where $\tilde{Q} \leqslant \tilde{Q}_{cr}$, the self-induced temperature perturbation is sufficiently small and no correction is needed. Figure 9a shows the plot of critical heat flux $\tilde{Q}_{cr}$ plotted for three

accuracy levels of $\beta = 0.1$, 0.01 and 0.001. For quick estimation, sometimes it is more convenient to only compare with the following asymptotic values of the critical heat flux

$$\tilde{Q}_{\rm cr}(\beta, {\rm Pe}_\sigma) = \begin{cases} \dfrac{(2\pi)^{3/2}\beta}{{\rm Pe}_\sigma} & \text{for} \quad {\rm Pe}_\sigma \ll 1 \\ 4\pi\beta & \text{for} \quad {\rm Pe}_\sigma \gg 1\,. \end{cases} \tag{38}$$

The asymptotic solutions indicate that the self-induced temperature correction criterion is more stringent in the high Pe_σ limit, where it is only dependent of β. The critical heat flux increases for lower Pe_σ indicating that the need for correction is easier to be avoided.

One can also transform the above criterion into a simple relation between more natural variables by substituting the non-dimensional thermal point-particle model $\tilde{Q}_{\rm cr} = 2\pi d^2 \Phi_T({\rm Re}_p, {\rm Pr}_f)/{\rm Pe}$. Here we assume the total heat flux is only due to the quasi-steady term with the finite Reynolds number correction function such as $\Phi_T({\rm Re}_p, {\rm Pr}_f) = 1 + 0.3\,{\rm Re}^{1/2}\,{\rm Pr}^{1/3}$ [25, 26]. The above thermal correction is similar to the finite Re standard drag correction. Then Figure 9b shows the critical non-dimensional particle diameter with respect to the particle Peclet number Pe. For small Peclet number we observe the asymptotic behavior to be $(d_*/\sigma_*)_{\rm cr} \sim \sqrt{2\pi\beta}$, while in the large Peclet limit the asymptotic behavior becomes $(d_*/\sigma_*)_{\rm cr} \sim \sqrt{2\beta\,{\rm Pe}}$. For example, if one chooses a Gaussian filter width such that $\delta_*/d_* = 2$ (or equivalently $d_*/\sigma_* \approx 1.18$), then from the figure it can be inferred that for 10% accuracy, the self-induced temperature correction is required when ${\rm Pe} < 6.93$. Instead if one requires a higher accuracy of 1% then the correction model is needed when ${\rm Pe} < 69.3$.

The criterion for the unsteady correction model mainly depends on the rate of change of the undisturbed temperature. From figure 7 we can draw a preliminary conclusion that the quasi-steady model is accurate enough if the undisturbed temperature varies slowly with $\tilde{\tau}_\theta > 10$ for $\mathrm{Pe}_\sigma < 1$. A weak dependence on Pe_σ can be observed. With increasing Pe_σ higher values of $\tilde{\tau}_\theta$ are required for unsteady effects to be unimportant, otherwise the unsteady model is required. Figure 8 shows the maximum absolute error in predicting the self-induced temperature using the two models. It indicates that the importance of unsteady model increases with decreasing $\tilde{\tau}_\theta$ and increasing Pe_σ. Also over the range of $\tilde{\tau}_\theta$ and Pe_σ values shown in Figure 8, unsteady model is needed in order to achieve 1% accuracy at all times. The corresponding conditions for Pe and St_{th} then depend on the value of σ_*/d_*.

7.1. Self-Induced Correction of Other Thermal Contributions

As seen in Figure 2, the thermal perturbation field induced by the Gaussian heat source/sink has a complex spatial structure. In an EL simulation, the simplest estimate of the heat exchange between the particle and the surrounding flow is using the quasi-steady heat transfer. This contribution depends on the difference between the point-particle temperature and the fluid temperature evaluated at the location of particle center. Thus, our attention has so far been focused on evaluating the self-induced perturbation to fluid temperature at the location of particle center. However, there are applications where the estimate of heat exchange between the particle and the surrounding must include contributions from other heat transfer mechanisms. A rigorous derivation [27] yields the following expression for the heat exchange between the spherical particle and the surrounding fluid

$$Q_* = 2\pi\lambda_* d_* \left(T_{p*} - \left[\overline{T}_*\right]_p - \frac{1}{24} d_*^2 \left[\nabla^2 \overline{T}_*\right]_p \right) - m_{f*} c_{p*} \left[\frac{D\overline{T}_*}{Dt_*}\right]_p , \tag{39}$$

where T_{p*} is the particle temperature, and m_{f*} is the mass of fluid displaced by the particle volume. The above expression ignores the history effect. The self-induced correction models of the fluid temperature at the particle location, $\left[\overline{T}_*\right]_p$, presented in the previous sections aims at obtaining accurate

predictions of only the quasi-steady contribution, $2\pi\lambda_* d_* \left(T_{p*} - \left[\overline{T}_*\right]_p\right)$. The factor $d_*^2 \left[\nabla^2 \overline{T}_*\right]_p /24$ in the first term accounts for the spatial variation in the fluid temperature over the size of the particle, and is known as the Faxén correction. The second term is the undisturbed flow heat transfer and is analogous to the undisturbed flow force in the point-particle force model.

We will now evaluate these additional contributions arising from the self-induced thermal field. We will restrict attention to the steady Oseen limit. The expression of $\left[\overline{T}_*\right]_p$ has already been discussed in Appendix A. Similar expressions of the local temperature Laplacian $\left[\nabla^2 \overline{T}_*\right]_p$ and advection $\left[D\overline{T}_*/Dt\right]_p$ are presented in Appendix B. The importance of self-induced temperature Laplacian (Faxén correction) can be evaluated by the ratio

$$r1 = \frac{d_*^2 \left[\nabla^2 \overline{T}_*\right]_p /24}{\left[\overline{T}'_*\right]_p} = -\frac{1}{24} \frac{\Psi_{\mathrm{TLap}}}{\Psi_{\mathrm{Tos}}} \left(\frac{d_*}{\sigma_*}\right)^2 . \tag{40}$$

And the effect of undisturbed flow heat flux with respect to the self-induced quasi-steady heat flux is obtained as

$$r2 = \frac{m_{f*} c_{p*} \left[\overline{u}_* \dfrac{\partial \overline{T}_*}{\partial x_*}\right]_p}{2\pi\lambda_* d_* \left[\overline{T}'_*\right]_p} = \frac{1}{36} \frac{\mathrm{Pe}_\sigma^2 \, \Psi_{\mathrm{Tadv}}}{\Psi_{\mathrm{Tos}} \, \phi_0} \left[1 - \frac{\mathrm{Pe}_\sigma \, F}{3\pi\sqrt{2\pi}} \Psi_{\mathrm{os}}\right] \left(\frac{d_*}{\sigma_*}\right)^2 , \tag{41}$$

where the temperature substantial derivative has been replaced by streamwise thermal advection. For estimation purposes, we assume Pr = 1 and have replaced Re_σ with Pe_σ in the above equation.

Figure 10 plots the three terms Ψ_{Tos}, Ψ_{TLap} and Ψ_{Tadv}. In the small Peclet number regime ($\mathrm{Pe}_\sigma \ll 1$), all three terms converge to unity. While in the finite Peclet number regime ($\mathrm{Pe}_\sigma \gg 1$), Ψ_{Tos} and Ψ_{TLap} decay at almost the same rate, but Ψ_{Tadv} decays much faster. Figure 11 shows the heat flux ratio of Faxén's correction and undisturbed heat transfer terms compared to the quasi-steady component. The ratios are calculated by setting the ratio $d_*/\sigma_* = 0.1$. Since Ψ_{Tos} and Ψ_{TLap} are comparable in magnitude, the effect of Faxén's correction can be considered solely influenced by d_*/σ_* and negligible in most cases. It should be noted that Faxén's correction may be of significance if the Gaussian filter width is chosen comparable to particle diameter. Similarly, the advection correction is also directly influenced by d_*/σ_*, but it increases with increasing Pe_σ because of the component $\mathrm{Pe}_\sigma^2 \, \Psi_{\mathrm{Tadv}}/\Psi_{\mathrm{Tos}}$. Result indicates that the advection correction can be ignored compared to the self-induced temperature correction for $\mathrm{Pe}_\sigma < O(100)$. For larger Peclet number the Oseen approximation used in the present analysis will not be valid. If the undisturbed temperature field changes rapidly, the effect of undisturbed heat flux can be further augmented. Besides, the feedback force does not play a salient role in evaluating $r2$. Increasing F from $O(1)$ to $O(10)$ will only slightly decrease $r2$. It can be concluded that over a wide range of Peclet number, the self-induced temperature correction is the most important factor to be considered.

8. Conclusion

In a two-way coupled Euler-Lagrange simulation, if the particle size is considerably smaller than the grid resolution, then the modification of the flow due to interphase back coupling of momentum and energy from that individual particle to the fluid is generally small (however the collective effect of many particles located within the grid can be significant). This is however not true when the particle diameter becomes comparable to the grid size. In this limit, the local fluid field is substantially

perturbed by the point particle. This perturbation at the particle center is defined as the self-induced velocity perturbation $\left[\overline{\mathbf{u}}'_*\right]_p$ due to momentum coupling and self-induced temperature perturbation $\left[\overline{T}'_*\right]_p$ due to energy coupling.

The thermal point-particle model depends on the temperature difference of the particle and the local undisturbed flow. However, the undisturbed flow temperature is unavailable in a two-way coupled Euler-Lagrange simulation, since the temperature interpolated to the particle center is already perturbed by the self-induced temperature. In this paper, we develop an explicit model to calculate the self-induced temperature perturbation, so that the undisturbed temperature can be recovered to improve the accuracy of the heat flux computation. This self-induced thermal correction model can be implemented in any two-way coupled Euler-Lagrange simulation.

The self-induced temperature perturbation is derived analytically from the Oseen's equation in the quasi-steady limit and Stokes equation in the unsteady limit. These analytical solutions strictly apply only in the limit $\mathrm{Re}_\sigma \to 0$ and $\mathrm{Pe}_\sigma \to 0$. Note that in an Euler-Lagrange simulation the only length scale of direct relevance is the width of the Gaussian filter function used to apply the momentum and energy back on the fluid from the particle. The Reynolds and Peclet numbers are therefore defined in terms of the Gaussian width. In the finite Reynolds/Peclet regime the self-induced temperature was obtained through numerical simulations. The simulation data shows that the analytical solutions are quite accurate even in the finite Peclet regime. Only a modest correction factor χ_T is needed to accurately fit the simulation results. The correction model primarily depends on three quantities: the feedback heat flux from particle to fluid Q_*, Gaussian Peclet number Pe_σ and the non-dimensional feedback force $\tilde{F} = |\mathbf{F}_*|/(\rho_* U_*^2 \sigma_*^2)$. Specifically, the thermal correction is linear in Q_*, while Pe_σ and $\tilde{F}$ account for the nonlinear effect. The correction model is also influenced by the numerical parameter δ_*/d_* which measures the number of grid points used to resolve the Gaussian filter. Provided $\delta_*/d_* \gtrapprox 4$ the results are insensitive to this parameter [1].

In problems where the momentum and thermal feedback to the fluid vary slowly in time, the steady correction model can be applied at each time instance in a quasi-steady manner to accurately predict the self-induced temperature. In problems where the time scale of temporal variation of momentum and energy feedback is short, unsteady effects become important. In this case, the quasi-steady prediction model is inadequate and an unsteady correction model is required. Here we combine the analytical unsteady model of the Stokes limit with the numerical simulation results in the unsteady regime to develop an unsteady self-induced velocity correction model.

The accuracy of the quasi-steady and unsteady models were tested over a wide range of Gaussian Peclet number ($\mathrm{Pe}_\sigma \lesssim 10000$), feedback force ($\tilde{F} \lesssim 3.5$), and non-dimensional timescales of thermal variation $\tilde{\tau}_\theta$. Though the correction models themselves depend only on the Gaussian width, the physical parameters of relevance are particle Peclet number and thermal Stokes number, which are related to Pe_σ and $\tilde{\tau}_\theta$. The unsteady model was able to accurately track the self-induced thermal perturbation even in cases of rapidly varying temperature of the undisturbed ambient flow. Thus, in any given physical problem characterized by Pe and St_{th}, the corresponding EL simulation parameters Pe_σ and $\tilde{\tau}_\theta$ can be evaluated from the choice of σ_*/d_*. These values can then be used to decide the need for quasi-steady or unsteady self-induced thermal correction.

We also provide simple criterion for when the self-induced temperature correction is needed in an Euler-Lagrange simulation. One can assess whether the correction is needed in terms of the feedback heat flux Q_*, Peclet number Pe_σ and the desired error tolerance β for the thermal point-particle model.

We have obtained an explicit expression for the critical non-dimensional heat flux $\tilde{Q}_{cr}$ as a function of Peclect number and β, and if the feedback heat flux exceed the critical value then self-induced thermal correction is required. For practical implementation, this criterion has been specialized for quasi-steady heat transfer from a rigid particle and restated in terms of critical value of the ratio d_*/σ_*, as a function of particle Peclet number Pe and β. The importance of the unsteady model increases with decreasing $\tilde{\tau}_\theta$ and increasing Pe_σ. Figure 8 can be used to evaluate the need for unsteady model for a desired level of accuracy.

The limitations for the correction model can be summarized as follows: (i) The correction is limited to incompressible assumption. (ii) The feedback force and heat flux are applied with a Gaussian filter and therefore the present correction model cannot be directly applied to other approaches of back coupling. However with a suitable modification the present results can be used with other feedback approaches as well. (iii) The particle Biot number is assumed much smaller than unity. If the particle is large enough and its internal temperature distribution is non-uniform, the correction model may need to be revised accordingly. (iv) Finally, here we have assumed the fluid flow to be unaffected by the thermal field. Instead, if the temperature distribution affects the flow through either buoyancy effects or variable transport properties, then the feedback heat flux will alter both the self-induced velocity and temperature correction. Such complication is not considered in this work.

Appendix A. Oseen's approximation at finite Peclet number

Following section 4.1, the volume-weighted governing equations of the Oseen's approximation can be derived from the original equations (8), (9) and (10). Under Oseen's approximation the thermal equation decouples from the other two equations. By assuming steady state and ignoring Reynolds and residual stress terms, we have

$$U_{0*}\frac{\partial \overline{T}_{v*}}{\partial x_*} = \alpha_* \nabla_*^2 \overline{T}_{v*} + \frac{Q_*}{\rho_* c_{p*}}\,, \tag{A.1}$$

where the non-linear advection term has been linearized. Non-dimensionalizing the above using the inertial scales of section 3 we obtain

$$\frac{\partial \tilde{T}'_v}{\partial x} = \frac{1}{\mathrm{Pe}_\sigma}\nabla^2 \tilde{T}'_v + \tilde{Q}\,\tilde{G}\,. \tag{A.2}$$

The exact solution can be obtained in the Fourier space as

$$\hat{T}'_v(\mathbf{k}) = \frac{\tilde{Q}\,\mathrm{Pe}_\sigma\,\hat{G}(\mathbf{k})}{k^2 + \iota\,\mathrm{Pe}_\sigma\,k_1} = \frac{\tilde{Q}\,\mathrm{Pe}_\sigma}{(2\pi)^{3/2}}\,\frac{1}{k^2 + \iota\,\mathrm{Pe}_\sigma\,k_1}\exp\left(-\frac{k^2}{2}\right), \tag{A.3}$$

where $\mathbf{k}$ is the three-dimensional wavenumber, $k = |\mathbf{k}|$, and k_1 is the component in the $\mathbf{U}_{0*}$ direction. The real space solution at the particle center can be derived through inverse Fourier transform

$$\begin{aligned}\left[\tilde{T}'_v\right]_p &= \tilde{T}'_v(\mathbf{x}=0) = \frac{1}{(2\pi)^{3/2}}\iiint_{-\infty}^{\infty}\hat{T}'_v(\mathbf{k})\;d\mathbf{k} \\ &= \frac{\tilde{Q}\,\mathrm{Pe}_\sigma}{(2\pi)^{3/2}}\Psi_{\mathrm{Tos}}\left(\mathrm{Pe}_\sigma\right)\,,\end{aligned} \tag{A.4}$$

where

$$\Psi_{\mathrm{Tos}}\left(\mathrm{Pe}_\sigma\right) = \sqrt{\frac{\pi}{2}}\;\frac{1-\exp\left(\dfrac{\mathrm{Pe}_\sigma^2}{2}\right)\cdot\mathrm{erfc}\left(\dfrac{\mathrm{Pe}_\sigma}{\sqrt{2}}\right)}{\mathrm{Pe}_\sigma}\,. \tag{A.5}$$

The asymptotic form of Ψ_{Tos} can be easily obtained by series expansion

$$\Psi_{\text{Tos}}\left(\text{Pe}_\sigma\right) = \begin{cases} 1 - \dfrac{\sqrt{\pi}\,\text{Pe}_\sigma}{2\sqrt{2}} + \dfrac{\text{Pe}_\sigma^2}{3} - \dfrac{\sqrt{\pi}\,\text{Pe}_\sigma^3}{8\sqrt{2}} + \dfrac{\text{Pe}_\sigma^4}{15} + O(\text{Pe}_\sigma^5) & \text{for} \quad \text{Pe}_\sigma \to 0 \\ \sqrt{\dfrac{\pi}{2}}\dfrac{1}{\text{Pe}_\sigma} - \dfrac{1}{\text{Pe}_\sigma^2} + \dfrac{1}{\text{Pe}_\sigma^4} + O(\dfrac{1}{\text{Pe}_\sigma^6}) & \text{for} \quad \text{Pe}_\sigma \to \infty \end{cases} . \tag{A.6}$$

When Pe_σ approaches zero, $\Psi_{\text{Tos}} \to 1$, which reduces to the Stokes solution. A plot of $\Psi_{\text{Tos}}\left(\text{Pe}_\sigma\right)$ is shown in Figure A.12.

If we assume the thermal feedback to be given by the quasi-steady component form the standard thermal point-particle model, i.e., if we assume $Q_* = -Q_{qs*} = -2\pi\lambda_* d_* T_{f*}\Phi(\text{Re}_p, \text{Pr}_f)$, then the perturbed temperature at particle center equals

$$\left[\overline{T}_*\right]_p = \frac{T_{f*}}{\phi_0}\left[1 - \frac{\Phi(\text{Re}_p, \text{Pr}_f)\Psi_{\text{Tos}}\left(\text{Pe}_\sigma\right)}{\sqrt{2\pi}}\frac{d_*}{\sigma_*}\right], \tag{A.7}$$

which includes Oseen's correction to the Stokes result given in equation (22).

Appendix B. Temperature Laplacian and advection

Following the derivation of (A.4), the temperature Laplacian can be obtained by performing the derivatives in Fourier space as

$$\begin{aligned} \left[\nabla^2\overline{T}\right]_p &= \frac{1}{(2\pi)^{3/2}\phi_0}\iiint_{-\infty}^{\infty} |\iota\mathbf{k}|^2\hat{T}'_v(\mathbf{k})\,\mathrm{e}^{\iota\mathbf{k}\cdot 0}\,d\mathbf{k} \\ &= -\frac{\tilde{Q}}{(2\pi)^2\phi_0}\int_0^\infty\int_0^\pi \frac{k^3\sin\theta}{\dfrac{k}{\text{Pe}_\sigma} + \iota\cos\theta}\exp\left(-\frac{k^2}{2}\right)\,d\theta dk\,. \end{aligned} \tag{B.1}$$

Here we assume the undisturbed temperature field to be uniform, and thus the Laplacian of temperature is equivalent to the Laplacian of perturbation temperature. To simplify the derivation, we assume $\nabla\phi \approxeq 0$ so that we can ignore the influence of volume fraction variation and only keep the leading order term $\left[\nabla^2\overline{T}\right]_p = \dfrac{1}{\phi_0}\left[\nabla^2\overline{T}_v\right]_p$. The final expression can be written as

$$\left[\nabla^2\overline{T}\right]_p = -\frac{\tilde{Q}\,\text{Pe}_\sigma}{(2\pi)^{3/2}\phi_0}\Psi_{\text{TLap}}(\text{Pe}_\sigma)\,. \tag{B.2}$$

The asymptotic solutions of Ψ_{TLap} can be expanded as

$$\Psi_{\text{TLap}}\left(\text{Pe}_\sigma\right) = \begin{cases} 1 - \dfrac{\text{Pe}_\sigma^2}{3} + \dfrac{\sqrt{2\pi}\,\text{Pe}_\sigma^3}{8} - \dfrac{\text{Pe}_\sigma^4}{5} + O(\text{Pe}_\sigma^5) & \text{for} \quad \text{Pe}_\sigma \to 0 \\ \dfrac{\sqrt{2\pi}}{\text{Pe}_\sigma} - \dfrac{3}{\text{Pe}_\sigma^2} + \dfrac{5}{\text{Pe}_\sigma^4} + O(\dfrac{1}{\text{Pe}_\sigma^6}) & \text{for} \quad \text{Pe}_\sigma \to \infty\,. \end{cases} \tag{B.3}$$

Similarly, to evaluate the advection term, first the streamwise component of temperature gradient can be calculated as

$$\begin{aligned}\left[\frac{\partial \overline{T}}{\partial x}\right]_p &= \frac{1}{(2\pi)^{3/2}\phi_0}\iiint_{-\infty}^{\infty}(\iota k_1)\hat{T}'_v(\mathbf{k})\,\mathrm{e}^{\iota\mathbf{k}\cdot 0}\,d\mathbf{k} \\ &= \frac{\tilde{Q}}{(2\pi)^2\phi_0}\int_0^{\infty}\int_0^{\pi}\frac{\iota k^2 \sin\theta\cos\theta}{\frac{k}{\mathrm{Pe}_\sigma}+\iota\cos\theta}\exp\left(-\frac{k^2}{2}\right)\,d\theta dk\,, \end{aligned} \tag{B.4}$$

which yields

$$\left[\frac{\partial \overline{T}}{\partial x}\right]_p = \frac{\tilde{Q}\,\mathrm{Pe}_\sigma^2}{6\pi\sqrt{2\pi}\phi_0}\Psi_{\mathrm{Tadv}}(\mathrm{Pe}_\sigma)\,. \tag{B.5}$$

The asymptotic expressions of Ψ_{Tadv} are

$$\Psi_{\mathrm{Tadv}}\,(\mathrm{Pe}_\sigma) = \begin{cases} 1-\dfrac{3\sqrt{\pi}\,\mathrm{Pe}_\sigma}{4\sqrt{2}}+\dfrac{3\,\mathrm{Pe}_\sigma^2}{5}+O(\mathrm{Pe}_\sigma^3) & \text{for} \quad \mathrm{Pe}_\sigma \to 0 \\ \dfrac{3}{\mathrm{Pe}_\sigma^2}-\dfrac{3\sqrt{2\pi}}{\mathrm{Pe}_\sigma^3}+\dfrac{9}{\mathrm{Pe}_\sigma^4}+O(\dfrac{1}{\mathrm{Pe}_\sigma^6}) & \text{for} \quad \mathrm{Pe}_\sigma \to \infty\,. \end{cases} \tag{B.6}$$

In the steady state, substantial derivative of temperature can be simplified as the nonlinear advection term $\left[\dfrac{D\overline{T}}{Dt}\right]_p = \left[\overline{u}\dfrac{\partial \overline{T}}{\partial x}\right]_p$. If we assume Prandtl number to be 1 (i.e. $\mathrm{Re}_\sigma = \mathrm{Pe}_\sigma$) and substitute the self-induced velocity model from [1], the thermal advection term becomes

$$\left[\overline{u}\frac{\partial \overline{T}}{\partial x}\right]_p = \frac{\tilde{Q}\,\mathrm{Pe}_\sigma^2}{6\pi\sqrt{2\pi}\phi_0^2}\Psi_{\mathrm{Tadv}}\left[1-\frac{\mathrm{Pe}_\sigma\,F}{3\pi\sqrt{2\pi}}\Psi_{\mathrm{os}}\right]. \tag{B.7}$$

Acknowledgments

This work was sponsored by the Office of Naval Research (ONR) as part of the Multidisciplinary University Research Initiatives (MURI) Program, under grant number N00014-16-1-2617. This work was also partially supported and benefited from the U.S. Department of Energy, National Nuclear Security Administration, Advanced Simulation and Computing Program, as a Cooperative Agreement to the University of Florida under the Predictive Science Academic Alliance Program, under Contract No. DE-NA0002378.

References

[1] S. Balachandar, K. Liu, M. Lakhote, Self-induced velocity correction for improved drag estimation in euler–lagrange point-particle simulations, Journal of Computational Physics 376 (2019) 160–185.

[2] S. Balachandar, A scaling analysis for point–particle approaches to turbulent multiphase flows, International Journal of Multiphase Flow 35 (2009) 801–810.

[3] S. Balachandar, J. K. Eaton, Turbulent dispersed multiphase flow, Annual Review of Fluid Mechanics 42 (2010) 111–133.

[4] J. K. Eaton, Two-way coupled turbulence simulations of gas-particle flows using point-particle tracking, International Journal of Multiphase Flow 35 (2009) 792–800.

[5] C. Marchioli, A. Soldati, J. Kuerten, B. Arcen, A. Taniere, G. Goldensoph, K. Squires, M. Cargnelutti, L. Portela, Statistics of particle dispersion in direct numerical simulations of wall-bounded turbulence: results of an international collaborative benchmark test, International Journal of Multiphase Flow 34 (2008) 879–893.

[6] S. Subramaniam, Lagrangian–eulerian methods for multiphase flows, Progress in Energy and Combustion Science 39 (2013) 215–245.

[7] J. Capecelatro, O. Desjardins, An euler–lagrange strategy for simulating particle-laden flows, Journal of Computational Physics 238 (2013) 1–31.
[8] S. Elghobashi, G. Truesdell, On the two-way interaction between homogeneous turbulence and dispersed solid particles. i: Turbulence modification, Physics of Fluids A: Fluid Dynamics 5 (1993) 1790–1801.
[9] Y. Ling, S. Balachandar, M. Parmar, Inter-phase heat transfer and energy coupling in turbulent dispersed multiphase flows, Physics of Fluids 28 (2016) 033304.
[10] J. Horwitz, A. Mani, Accurate calculation of stokes drag for point–particle tracking in two-way coupled flows, Journal of Computational Physics 318 (2016) 85–109.
[11] T. Fukada, S. Takeuchi, T. Kajishima, Interaction force and residual stress models for volume-averaged momentum equation for flow laden with particles of comparable diameter to computational grid width, International Journal of Multiphase Flow 85 (2016) 298–313.
[12] T. Fukada, W. Fornari, L. Brandt, S. Takeuchi, T. Kajishima, A numerical approach for particle-vortex interactions based on volume-averaged equations, International Journal of Multiphase Flow 104 (2018) 188–205.
[13] G. Akiki, T. Jackson, S. Balachandar, Force variation within arrays of monodisperse spherical particles, Physical Review Fluids 1 (2016) 044202.
[14] G. Akiki, T. Jackson, S. Balachandar, Pairwise interaction extended point-particle model for a random array of monodisperse spheres, Journal of Fluid Mechanics 813 (2017) 882–928.
[15] Y. (Yali) Tang, E. (Frank) Peters, J. (Hans) Kuipers, S. (Sebastian) Kriebitzsch, M. (Martin) van der Hoef, A new drag correlation from fully resolved simulations of flow past monodisperse static arrays of spheres, AIChE journal 61 (2015) 688–698.
[16] P. Pakseresht, S. V. Apte, Volumetric displacement effects in euler-lagrange les of particle-laden jet flows, International Journal of Multiphase Flow 113 (2019) 16–32.
[17] P. Gualtieri, F. Picano, G. Sardina, C. M. Casciola, Exact regularized point particle method for multiphase flows in the two-way coupling regime, Journal of Fluid Mechanics 773 (2015) 520–561.
[18] P. J. Ireland, O. Desjardins, Improving particle drag predictions in euler–lagrange simulations with two-way coupling, Journal of Computational Physics 338 (2017) 405–430.
[19] J. Horwitz, A. Mani, Correction scheme for point-particle models applied to a nonlinear drag law in simulations of particle-fluid interaction, International Journal of Multiphase Flow 101 (2018) 74–84.
[20] M. Esmaily, J. Horwitz, A correction scheme for two-way coupled point-particle simulations on anisotropic grids, Journal of Computational Physics 375 (2018) 960–982.
[21] J. Horwitz, S. Ganguli, A. Mani, S. Lele, A correction procedure for thermally two-way coupled point-particles, in: APS Meeting Abstracts, 2017.
[22] P. F. Fischer, J. W. Lottes, S. G. Kerkemeier, et al., nek5000 web page, 2008, URL http (2008).
[23] Y. Chia-Shun, Fluid mechanics: a concise introduction to the theory, McGraw-Hill, 1969.
[24] R. Mei, R. J. Adrian, Flow past a sphere with an oscillation in the free-stream velocity and unsteady drag at finite reynolds number, Journal of Fluid Mechanics 237 (1992) 323–341.
[25] S. Whitaker, Forced convection heat transfer correlations for flow in pipes, past flat plates, single cylinders, single spheres, and for flow in packed beds and tube bundles, AIChE Journal 18 (1972) 361–371.
[26] W. Ranz, W. R. Marshall, et al., Evaporation from drops, Chem. Eng. Prog 48 (1952) 141–146.
[27] E. E. Michaelides, Z. Feng, Heat transfer from a rigid sphere in a nonuniform flow and temperature field, International journal of heat and mass transfer 37 (1994) 2069–2076.

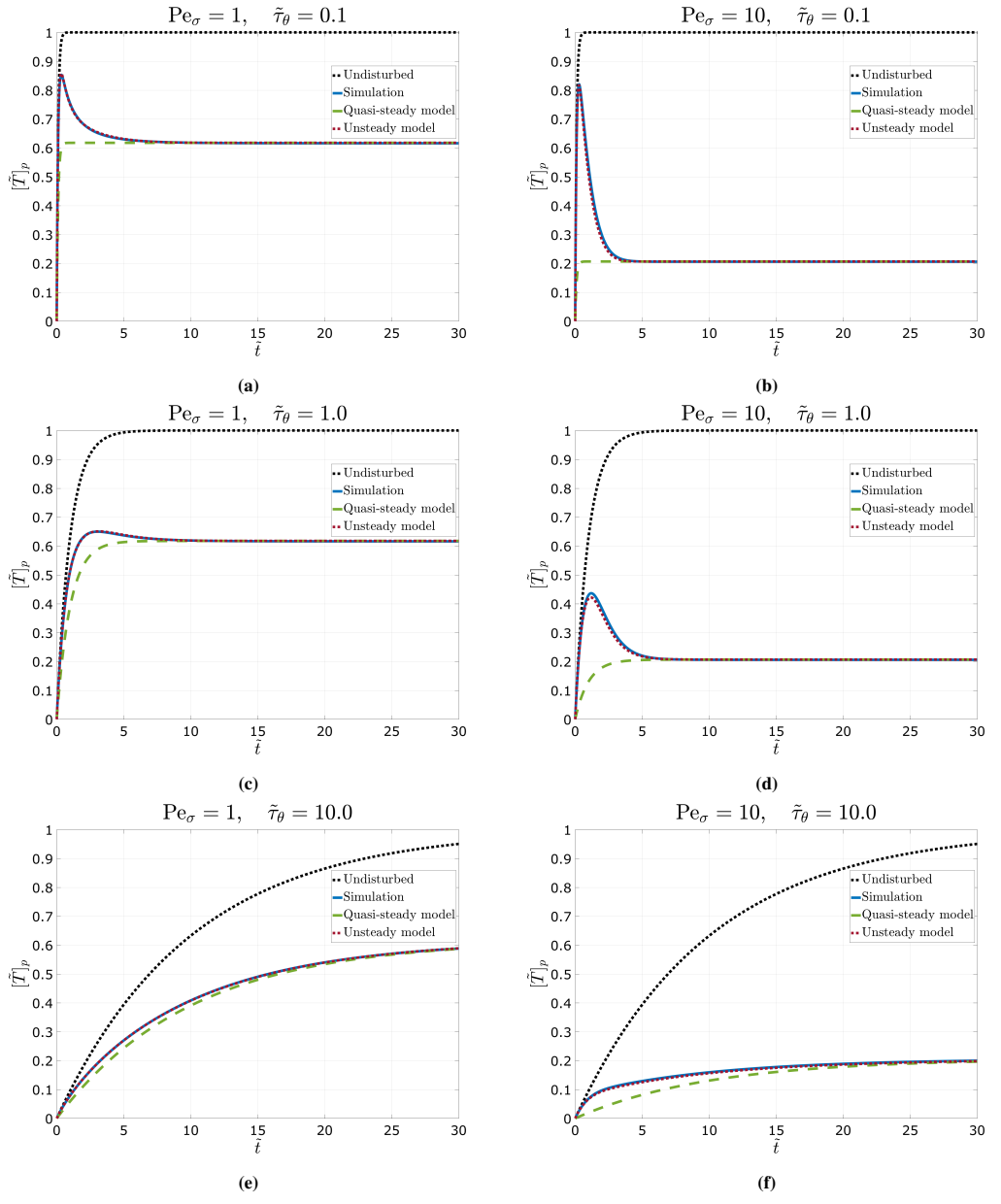

Fig. 7: Time evolution of the temperature values at the particle center. The black dotted line is the undisturbed temperature based on the far-field flow (35). The blue line is the temperature from numerical simulations. The explicit predictions by the quasi-steady and unsteady correction models are represented by the green and red lines respectively. The six cases are: (a)$\mathrm{Pe}_\sigma = 1$, $\tilde{\tau}_\theta = 0.1$; (b)$\mathrm{Pe}_\sigma = 10$, $\tilde{\tau}_\theta = 0.1$; (c)$\mathrm{Pe}_\sigma = 1$, $\tilde{\tau}_\theta = 1$; (d)$\mathrm{Pe}_\sigma = 10$, $\tilde{\tau}_\theta = 1$; (e)$\mathrm{Pe}_\sigma = 1$, $\tilde{\tau}_\theta = 10$; (f)$\mathrm{Pe}_\sigma = 10$, $\tilde{\tau}_\theta = 10$.

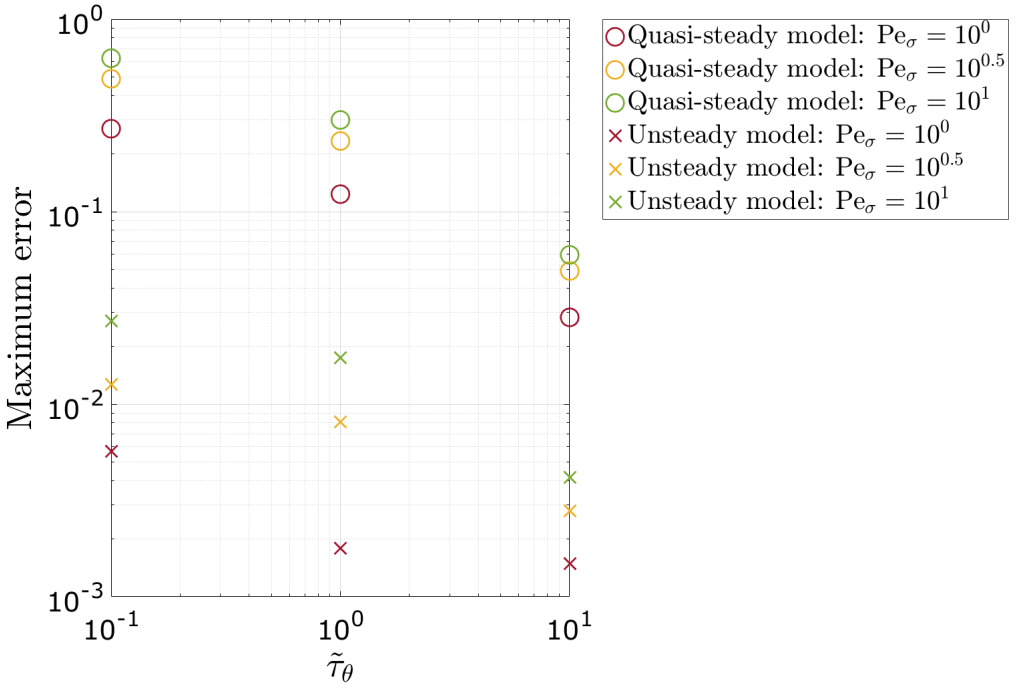

Fig. 8: Plot of the maximum absolute error in predicting the self-induced temperature using quasi-steady (circles) and unsteady (crosses) models.

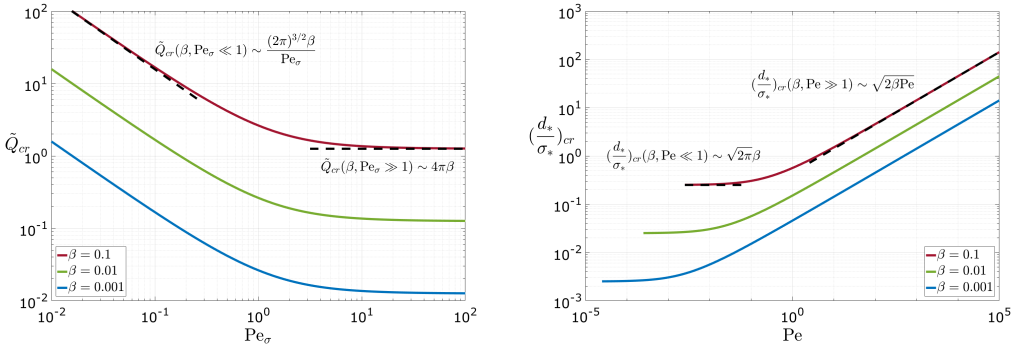

(a) **(b)**

Fig. 9: Critical values in three accuracy levels β=0.1, 0.01 and 0.001. (a) Critical heat flux $\tilde{Q}_{cr}$ with respect to Gaussian Peclet number Pe_σ. (b) Critical non-dimensional diameter $(\frac{d_*}{\sigma_*})_{cr}$ with respect to Particle Peclet number Pe.

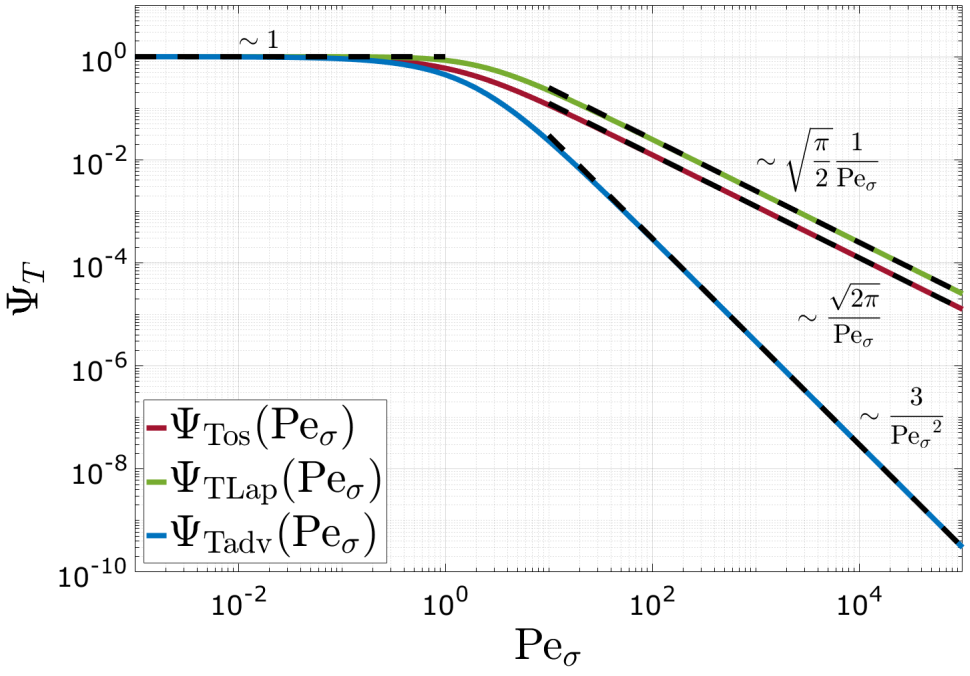

Fig. 10: Plot of analytical terms Ψ_{Tos}, Ψ_{TLap} and Ψ_{Tadv}, as well as their asymptotic leading order components in the zero and infinity limits.

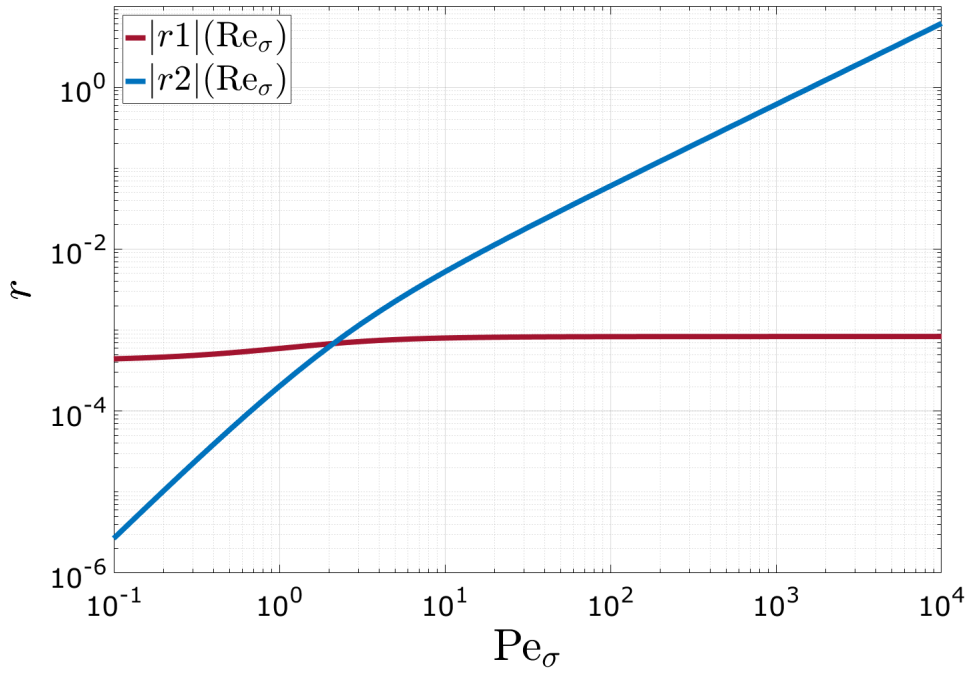

Fig. 11: Plot of heat flux ratio of Faxen's correction and undisturbed term compared to the quasi-steady component due to self-induced temperature. Here we assume diameter ratio $d_*/\sigma_* = 0.1$, Prandtl number $\mathrm{Pr} = 1$ and feedback force magnitude $F = 1$.

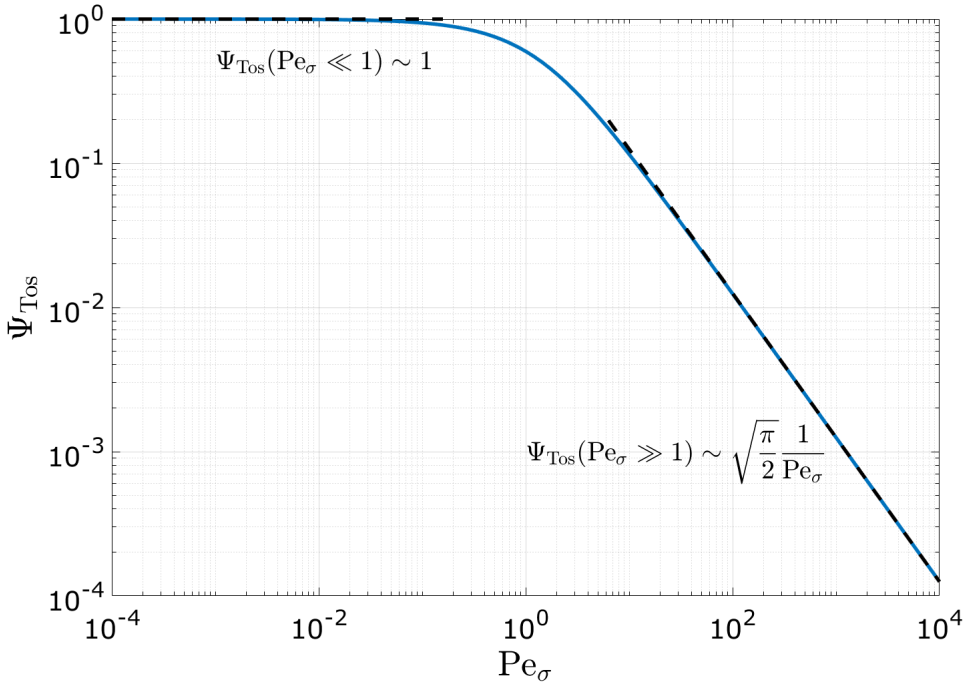

Fig. A.12: Plot of Ψ_{Tos} along with the asymptotic solutions.